

### **SECTION 3: MODEL INITIALIZATION**

### 3) Model Initialization

Altogether there are seven primary variables that enter into a solution for the simultaneous dispersion and dilution of the waste heat from the generating station and concentrated seawater from the desalination plant. These seven variables may be organized into *boundary conditions* and *forcing functions*. The boundary condition variables control the source strength (concentrated sea salts) and background conditions. Some of these change daily (primary boundary conditions) while others vary slowly in time (stationary boundary conditions). The primary boundary conditions are:

- \*Power Plant Flow Rates
- \*Ocean Salinity
- \*Ocean Temperature
- \*Ocean Water Levels (tides and sea level anomalies)

Storm water flows (such as from the Santa Ana River and Talbert Marsh) also vary daily, but their effect on the receiving water is captured by the daily ocean salinity data. However for the purpose of providing input to the Sanitary Survey (Archibald, 2002, 2004) we will consider their source loading during extreme events (see Sections 7 & 8). Similarly, the generating station “Delta-T” (the amount that the generating station raises the cooling water above the ambient ocean temperature) is added to the daily variation in ambient ocean temperature. The stationary boundary conditions are the local bathymetry, that typically has seasonal variation inshore of closure depth (about 15 m depth). The forcing function variables affect the strength of ocean mixing and ventilation and include:

- \* waves
- \* currents
- \*winds.

In the following sub-sections, overlapping 20.5 year long records for each of the seven controlling variables are reconstructed. These long-term records contain 7,523 consecutive days of daily mean values between 1980 and 2000.

Long-term monitoring of ocean properties in the coastal waters surrounding AES Huntington Beach has been on going for about 30 years as required for compliance with NPDES permits for two separate ocean outfalls, namely, the thermal outfall of AES Huntington Beach and the treated sewage outfall offshore of the Santa Ana River operated by Orange County Sanitation Department (OCSD). These data were accessed from the NPDES monitoring reports that are periodically released (MBC 1980- 2002 for the AES Huntington Beach outfall and OCSD,1993, 2000 for the OCSD outfall). In attempting to reconstruct 20-year long, continuous, unbroken records of all seven controlling variables for the dilution and dispersion modeling problem, certain gaps were found in some of the data bases. These gaps were filled by using monitoring data measured at the Scripps Pier in La Jolla, about 67.7 miles to the southeast of AES Huntington Beach . The Scripps Pier site has many physical features in common with the nearshore area around AES Huntington Beach. Both sites have a submarine canyon nearby. Consequently internal waves are an active mechanism at both sites in causing daily (diurnal) variations in salinity, temperature, and other ocean properties. The longer period variations at seasonal and multiple year time scales are the same at both sites due to their proximity. Consequently the Scripps Pier Shore Station data (SIO, 2001) and the Coastal Data Information Program monitoring at Scripps Pier (CDIP, 2004) are

used as surrogates to fill gaps in the long term records of physical ocean properties at AES Huntington Beach. These properties will be shown to exhibit considerable natural variability over the period of record from 1980 to mid 2000 due to daily and seasonal changes, but most especially due to climate changes of global scale.

The seasonal variations in the exposure of the hemispheres to the sun produce inter-annual changes in the duration of daylight and the angle of the sun's irradiance. These effects modulate solar heating, resulting in the inter-annual variation of the earth's atmospheric pressure field which in turn introduces seasonal climatic effects. Inter-annual variations are enhanced by the higher convective effects of land and the greater concentration of land mass relative to water in the temperate latitudes of the northern hemisphere.

Upon occasion the typical seasonal weather cycles are abruptly and severely modified on a global scale. These intense global modifications are signaled by anomalies in the pressure fields between the tropical eastern Pacific and Malaysia known as the *El Niño/Southern Oscillation* (ENSO) (e.g., Diaz & Markgraf, eds., 1992). The intensity of the oscillation is often measured in terms of the *Southern Oscillation Index* (SOI), defined as the monthly mean sea level pressure anomaly in mb normalized by the standard deviation of the monthly means for the period 1951-1980 at Tahiti, minus that at Darwin, Australia. A negative SOI (lower pressure at Tahiti, higher pressure at Darwin) is known as an *El Niño* or warm ENSO event, because of the arrival of unusually warm surface water off the coast of Peru at the time of Christmas; hence, the term El Niño. Warm water also occurs along the coast of California and both regions experience unusually heavy rainfall. A positive SOI is known as *La Niña* and it signals the occurrence of colder than

normal surface water in the eastern Pacific, but stronger southwest monsoons in the Indian Ocean with heavy rainfall in India and in the Ethiopian plateau.

ENSO events occur about every 3 to 7 years with dominant spectral peaks at about 3 and 6 plus years. However these ENSO events may induce climate changes that occur on decadal time scales of one quarter to one half century. These changes are often discussed in terms of two atmospheric patterns (PNA, NAO) and a sea surface temperature pattern (PDO). Both PNA and PDO are long period (i.e., inter-decadal) analogs of the seasonal (inter-annual) variations of global pressure and temperature, while NAO is an intensification and relaxation of the January phase of the inter-annual variation. They are aliased by the inter-annual changes because they have the same structure and appear as extreme cases of the inter-annual patterns. This aliasing has delayed the general understanding and acceptance of these concepts.

The Pacific/North American (PNA) pattern is associated with an atmospheric dipole in pressure anomaly over the Pacific Ocean/North America region whose polarity reversals lead to wet and dry climate along the Pacific coast of North America (Wallace & Gutzler, 1981). High pressure anomaly over the North Pacific Ocean and low pressure anomaly over the North American Continent result in dry (La Niña) climate along the coast of central and southern California; while the opposite polarity in these longitudinal (zonal) dipole patterns leads to wet (El Niño) climate. Inman & Jenkins (1999) show that the coastal rivers of central and southern California have streamflow and sediment fluxes during the wet phase of PNA (1969-1995) that exceed those during the preceding dry phase (1944-1968) by factors of 3 and 5 respectively.

The Pacific (inter) Decadal Oscillation (PDO) is a sea surface temperature pattern associated with the La Niña/El Niño phases of ENSO cycles, with the leading pattern of PDO situated in the tropical Pacific Ocean (Goddard & Graham, 1997; Mantua et al., 1997). The El Niño phase of the PDO cycle is characterized by a weakening of the trade winds that results in an eastward movement (slosh) of the warm pool of equatorial water normally contained in the western Pacific by the trades during La Niña conditions. The stronger trade wind systems during the La Niña phase of PDO are part of a general spin-up of the atmospheric circulation which causes the North and South Pacific Gyres to rotate faster. Both effects (wind and current) induce upwelling that maintains cold water masses along the west coast of the Americas, which sustains the typically cool dry coastal climate of these regions during the La Niña dominated periods of the PDO and PNA.

#### **A) Storm Water Flow Rates**

The historic occurrences of major flood events on the Santa Ana River will dictate the ensemble of environmental forcing parameters used to initialize the model for evaluation of source water issues related to potential ingestion of storm water by the AES Huntington Beach infall. We seek the largest historic floods for which wave and tidal data are simultaneously available.

To determine the likely maximum contribution of storm flow from the Santa Ana River and the Talbert Channel at the intake to the desalination plant, a composite monthly flow rate record was constructed using historic peak flow events of both the Santa Ana River and the Talbert Channel. The USGS has published annual mean flow volumes since 1940 and daily event based runoff volumes for the Santa Ana River during water years 1997-98 and 1998-99 (USGS,

2000). The Santa Ana River stream gage station (USGS #11078000) has an upstream drainage area of 4,400 square kilometers. The annual mean flow volumes at gage #11078000 for 1940-99 are listed in Table 1.

Because the oceanographic conditions which control the dispersion of the Santa Ana River storm water vary daily, it is necessary to select an event year from Table 1 for which daily flow rate data is available. The largest event year for which such daily flow rate data is available was water year 1998, which is the fourth largest event year in the period of record. Within that year, the highest flow month was February which accounted for 330 million of the 407 million cubic meters of flow volume occurring in water year 1998. The peak flow event occurred 24 February 1998.

Corresponding daily flow rate data for the Talbert Channel was not available for February 1998. Therefore a surrogate drainage basin was adopted for which flow rate data was simultaneously available at other times for both the surrogate and the Talbert Channel. These simultaneous flow rate data sets were used to construct a streamflow rating function, which establishes an analytic relation between the flow rate of the surrogate and the flow rate of the Talbert Channel. The rating function has the following form

$$Q_T = a_0 + a_1 Q_s + a_2 Q_s^2 \quad (9)$$

where  $Q_T$  is the flow rate of the Talbert Channel,  $Q_s$  is the flow rate of the surrogate and  $a_0$ ,  $a_1$  and  $a_2$  are parameters determined by regression analysis of the simultaneous data sets. The San Diego Cr. was selected as the surrogate for this

**Table 1.** Annual Mean Flow Volume for the Santa Ana River, USGS #11078000.

<b>Water Year<sup>b</sup></b>	<b>Streamflow 10<sup>6</sup>m<sup>3</sup>/yr.</b>	<b>Water Year<sup>b</sup></b>	<b>Streamflow 10<sup>6</sup>m<sup>3</sup>/yr.</b>	<b>Water Year<sup>b</sup></b>	<b>Streamflow 10<sup>6</sup>m<sup>3</sup>/yr.</b>
1940	3.84	1965	1.25	1990	16.6
1941	104	1966	25.8	1991	52.7
1942	.714	1967	42.2	1992	55.3
1943	79.8	1968	9.02	1993	547
1944	20.2	1969	480	1994	4.64
1945	7.50	1970	2.86	1995	346
1946	3.48	1971	5.09	1996	7.71
1947	2.50	1972	5.63	1997	39.8
1948	.0893	1973	16.7	1998	407
1949	.000	1974	12.1	1999	5.22
1950	.804	1975	7.68		
1951	.0893	1976	3.57		
1952	20.5	1977	3.30		
1953	.625	1978	272		
1954	1.70	1979	33.5		
1955	.268	1980	498		
1956	4.64	1981	18.6		
1957	.179	1982	22.1		
1958	23.8	1983	344		
1959	.447	1984	49.1		
1960	.804	1985	48.6		
1961	.000	1986	79.4		
1962	5.00	1987	14.6		
1963	1.52	1988	25.5		
1964	1.16	1989	23.4		

analysis for the following reasons:

- 1) Daily flow rate data available for February 1998.
- 2) Geographic proximity.
- 3) Similar basin hydrology, land use and demographics.
- 4) Both basins discharge into coastal marshes.

The resulting streamflow rating function giving Talbert Channel flow from San Diego Cr. flow is shown in Figure 3.1. The measured flow rate data appear as crosses in this figure and the best fit line from the regression analysis gives  $a_0 = 0.0461156$ ,  $a_1 = 0.0166263$  and  $a_2 = -0.0000194$ . The r-squared for this regression is 0.78 to 0.79, which is typical precision for this type of approximation, (Inman and Jenkins, 2000).

Since the mouths of the Santa Ana River and the Talbert Channel are essentially co-located by a system of jetties (Figure 1.3) a composite flow rate history was generated (Figure 3.2) for use in the model problem to predict the source water make-up at the AES intakes. Inspection of Figure 3.2 indicates that the maximum daily flow rate was 8,890 cfs for the combined Santa Ana River and Talbert Channel flow (24 February 1998). The seven day average of the combined flow rate around the peak flow event was 5,798 cfs and the thirty day average flow rate for the composite extreme event month was 2,732 cfs. The in-plant waste stream of storm water from the AES Huntington Beach facilities during this same period had a peak daily discharge of 0.72689 mgd, a seven day peak period average of 0.4741 mgd and a 30-day average of 0.186552 mgd, (see Appendix A).

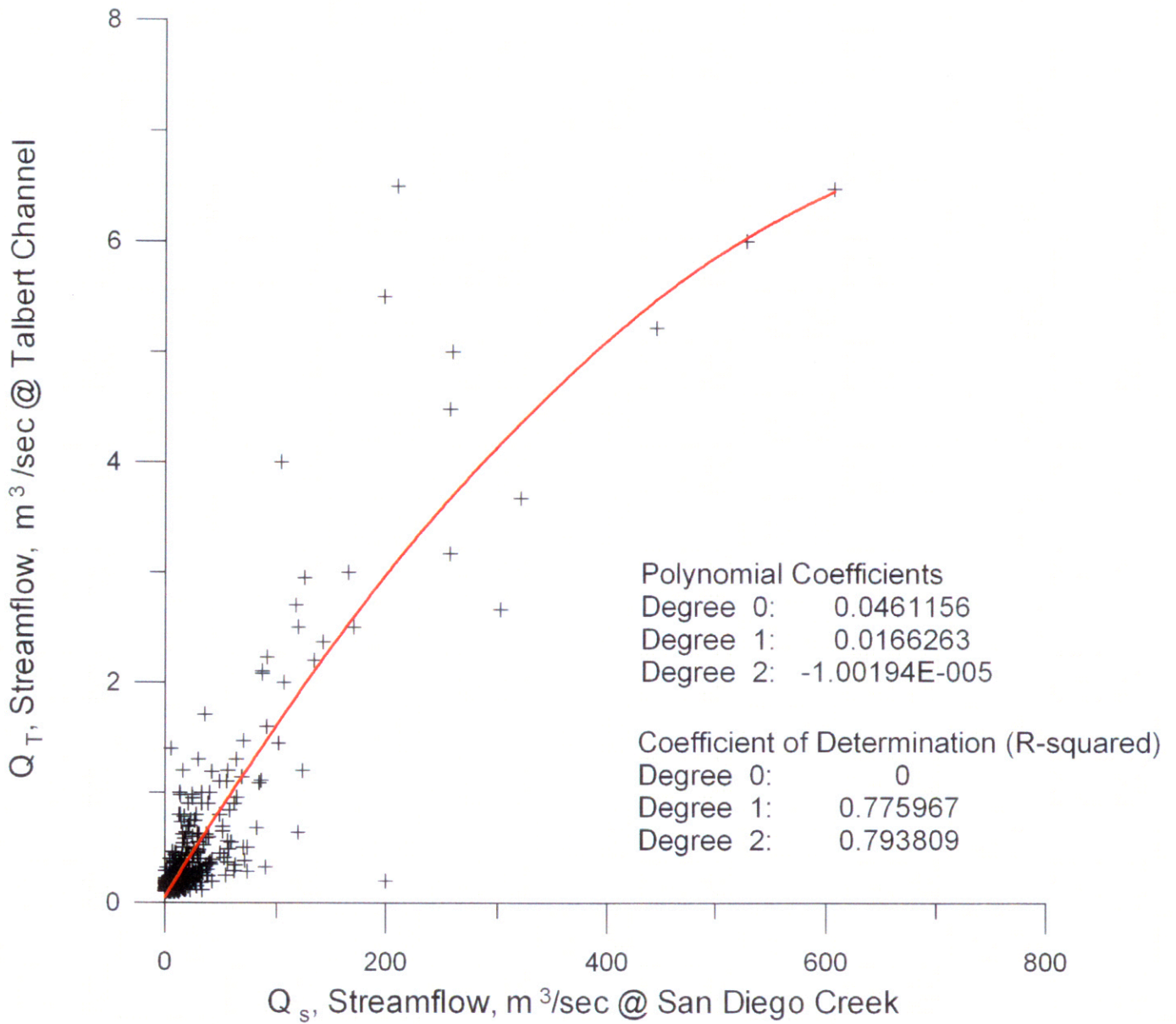


**Figure 3.1.** Talbert Channel streamflow rating function based on San Diego Creek surrogate.

## **B) Ocean Water Levels & Tidal Oscillations**

The local water depth around outfall of the AES Huntington Beach generating station is nominally 27.9 feet relative to mean sea level. Spring tidal ranges can reach as high as 8.9 feet or 32 % of the local mean water depth. Hence tides can significantly vary the local water volume around the outfall that is available for dilution. The nearest ocean tide gage station that measures ocean water levels near AES Huntington Beach is located at Newport Harbor. However this tide gage was not functional throughout the entire 1980-2000 period of record used for the modeling. Consequently the ocean water level input was de-faulted to the next closest tide gage station at Los Angeles (NOAA #941-0660). This tide gage was last leveled using the 1960-78 tidal epoch, but tide tables based on the 1960-78 tidal epoch frequently mis-represent high and low tide elevations. This is due to several factors including: 1) the long-term upward creep in eustatic sea level during the last part of the modern sea level high stand 2) seasonal warming and cooling of the ocean and 3) climate effects. Flick & Cayan (1984) have shown that seasonal warming and cooling accounts for an interannual variation in mean sea level of about 0.5 ft. El Niño or ENSO events can result in sea level anomalies of 1.0 ft. or more due to the thermal expansion effects of the coastal warm water anomalies of El Niño and by the inverse barometer effects on sea level associated with the ENSO induced North Pacific low pressure anomaly. Therefore, we base our analysis on direct water level measurements rather than on tide table estimates.

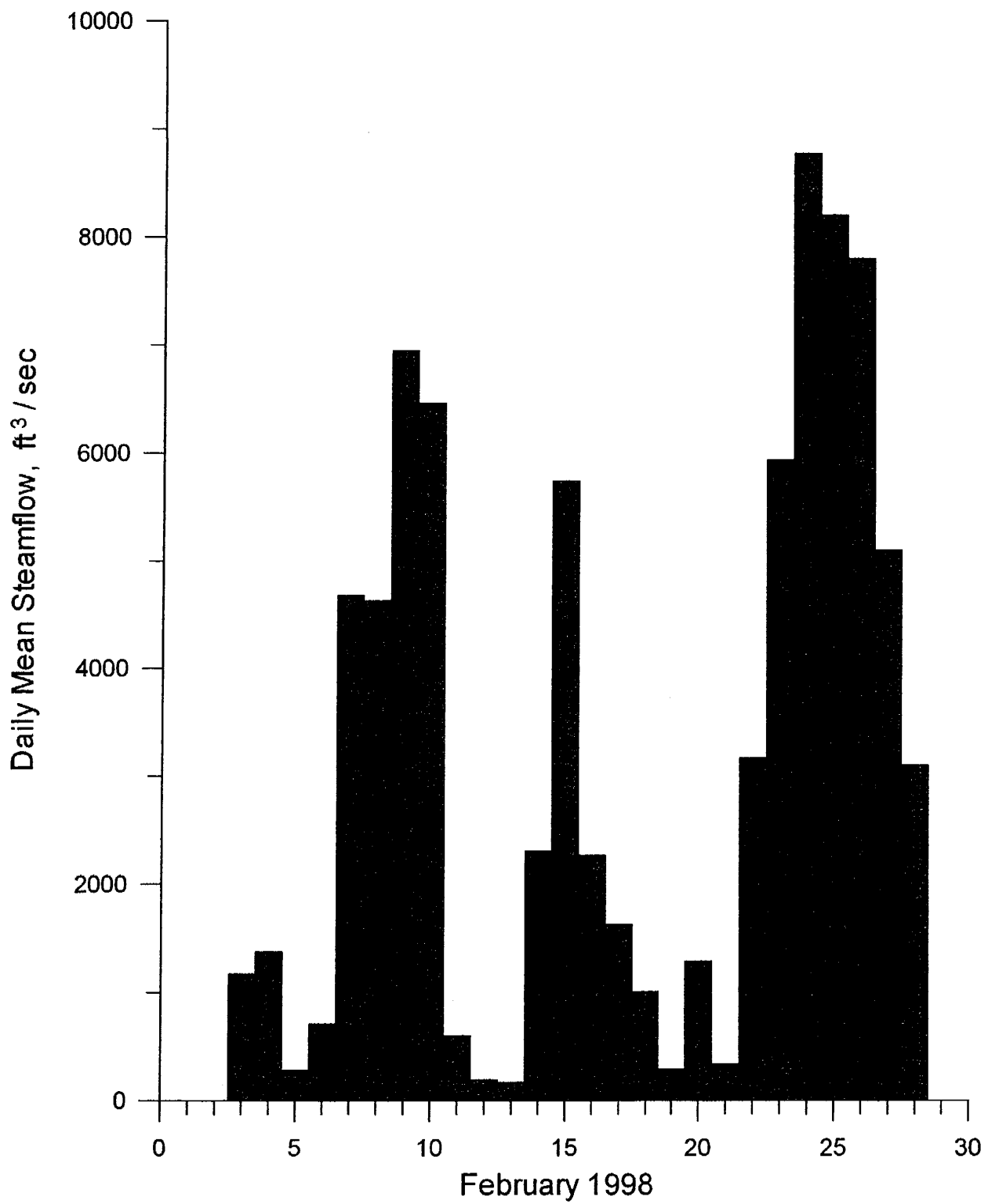


**Figure 3.2.** Combined daily mean flow rate of the Santa Ana River and Talbert Channel.

Water levels measured by the Los Angeles Tide Gage (NOAA #941-0660) have been archived by NOAA (2000) for the preceding 20.5 year period, 1980 through mid 2000. Time series of the daily high and low ocean water levels were reconstructed from these archival measurements for each year in this period of record. Here, tide measurements are recorded in one hour intervals. This sampling interval is too coarse to use these records directly as forcing functions for the tidal hydraulics computations. If the tidal flow becomes critical in any shallow water region of the model, by achieving the phase speed of a shallow water tidal wave,  $c = \sqrt{gh}$ , then the 2-dimensional Courant-Friedricks-Lewy (CFL) criterion (Gallagher, et al. 1981) is used as a generalized constraint to ensure stability of the finite element calculations. Some nodes must be closely spaced with  $\Delta x = 30$  m in order to resolve the geometry around the infall and outfall towers (Figure 1.2). The CFL criterion requires a minimum time step length:

$$\Delta t \leq \frac{\Delta x}{2c} \quad (10)$$

For a spring tide condition, maximum water depths could vary from 3 m to 7 m at certain sections of the infall and outfall towers. Therefore, the tidal forcing function must be resolved into time step intervals of less than 2.7 sec. if the tidal currents approached critical speeds in the channel at the Santa Ana River mouth or less than 3.2 sec. if critical flow was approached over the top of the infall and outfall towers.

The tides were reconstructed at 2 sec time intervals from the Los Angeles tidal measurements using the amplitudes and phases of 21 non-zero tidal constituents derived from the long-term records of the tide gage. This tidal reconstruction was performed by the program, **TID\_DAYS**, which is found in Appendix C. **TID\_DAYS** uses a version of LONG'S CODE from U. S. Dept. of Commerce SP #98\_1988. Figure 3.3 shows a comparison between the reconstructed tides at Los Angeles (solid line) versus the hourly measurements (triangles) for the tidal month of February 1998 used in the model problem for source water and dilution issues in Section 4. The tidal constituents for Los Angeles that were input to **TID\_DAYS** are based upon the NOAA datums derived from the 1960-78 tidal epoch. This was the last time that NOAA had updated datum elevations for the Los Angeles gage and corresponds to the predominant dry La Niña dominated period. Because of sea level anomalies due to El Niño warming of the coastal ocean, and inverse barometer effects due to storm passage, the reconstructed tides were assigned a positive sea level anomaly to minimize the variance between the measured water elevations in February 1998 and the reconstructed tides at 2 second intervals. That anomaly varied from +0.2 ft to +0.9 ft. during February 1998.

To initialize the model problem to study the transport of OCSD wastefield water masses during El Niño summer conditions in Section 9, the **TID\_DAYS** code in Appendix C was configured for 2 sec. time steps to reconstruct the tidal elevation during a period of reversal in the coastal transport. The wave record was searched for two to five day blocks having sustained reversals in the net littoral drift. The month of August 1997 was found to have the desired low flow case current reversals for investigating weather the OCSD waste field might reach the

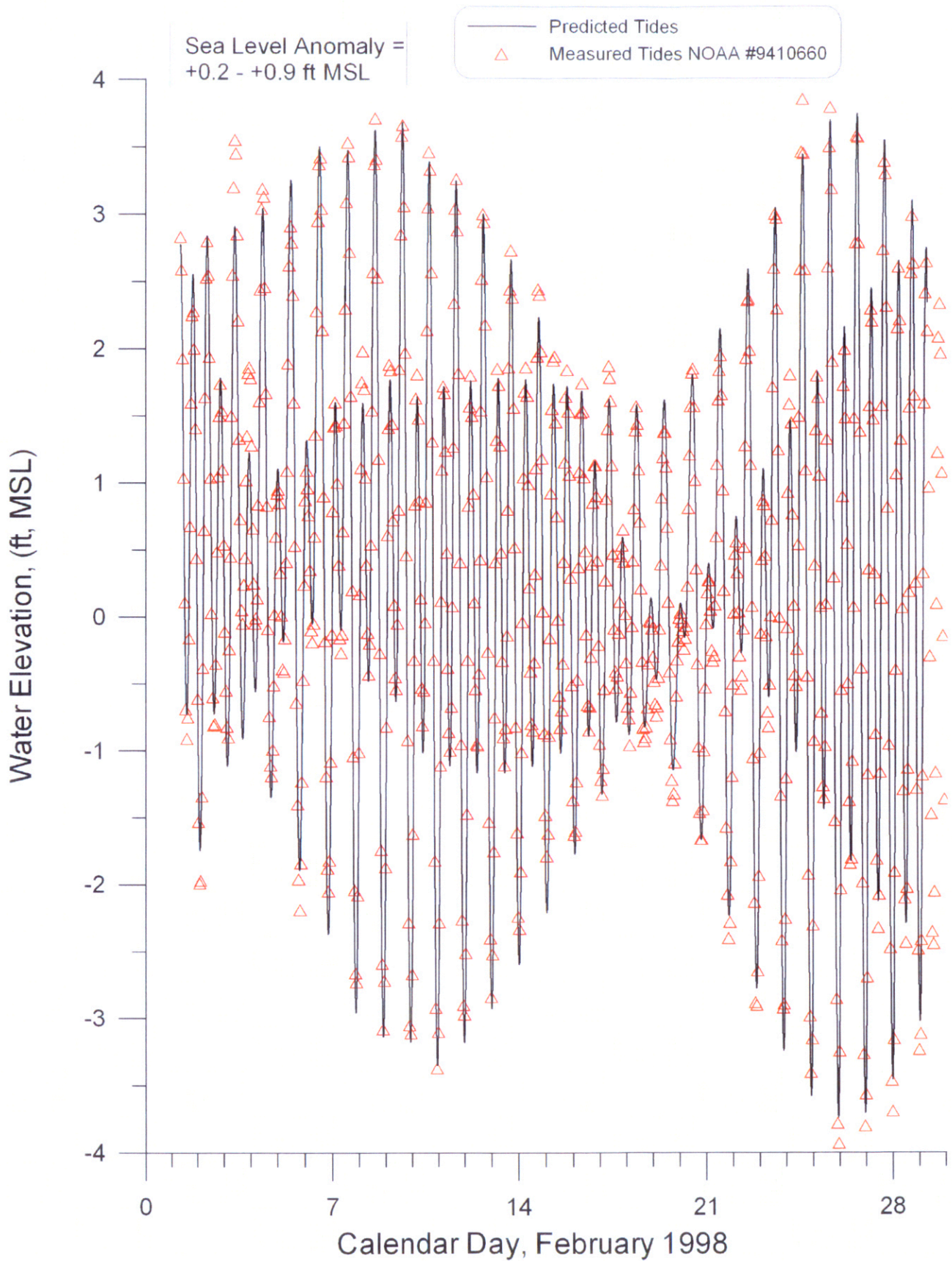


**Figure 3.3.** Predicted tides vs measured water levels at Los Angeles, CA, NOAA Tide gage #941-0660, February 1998.

AES intakes. The reconstructed water level elevation for August 1997 are shown in Figure 3.4. Similar reconstructions were done for the month of May during the La Niña year of 1999 to provide Syzygial tides with minimal tidal ranges for the low flow case dilution analysis in Section 4. The maximum ocean water level was +5.35 ft. NGVD during the 1997 El Niño, 1.31 ft. higher than the astronomic tides of the tide tables. The minimum ocean water level was -4.66 ft. NGVD, occurring during the 1988 winter. The 20.5 year record of daily high and low water levels is plotted in Panel-d of Figure 3.23 found at the end of this section, summarizing the complete set of boundary conditions.

### **C) Bathymetry**

Bathymetry provides a controlling influence on all of the coastal processes that affect dispersion and dilution. The bathymetry consists of two parts: 1) a stationary component in the offshore where depths are roughly invariant over time, and 2) a non-stationary component in the nearshore where depth variations do occur over time. The stationary bathymetry generally prevails at depths that exceed *closure depth* which is the depth at which net on/offshore transport vanishes. Closure depth is typically -12 m to -15 m MSL in the San Pedro Littoral Cell, [Inman et al. 1993]. The stationary bathymetry was derived from the National Ocean Survey (NOS) digital database. Gridding is by latitude and longitude with a 3 x 3 arc second grid cell resolution yielding a computational domain of 30.9 km x 18.5 km. Grid cell dimensions along the x-axis (longitude) are 77.2 meters and 92.6 meters along the y-axis (latitude).

For the non-stationary bathymetry data inshore of closure depth (less than -15 m MSL) nearshore and beach surveys were conducted by the US Army Corps

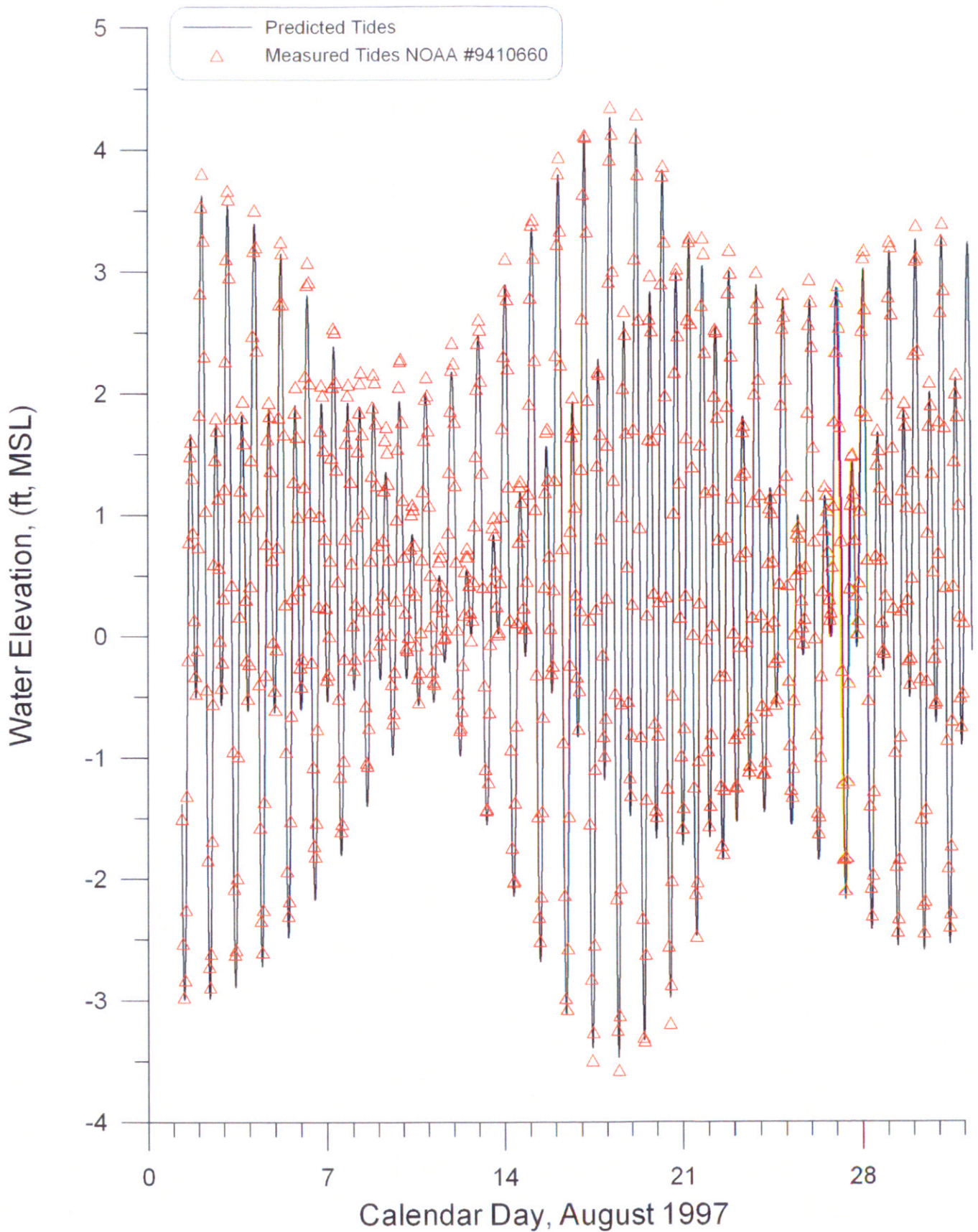


**Figure 3.4.** Predicted tides vs measured water levels at Los Angeles, CA, NOAA Tide gage #941-0660, August 1997.

of Engineers in 1985, 1990, 1996 and have been compiled in Everts, 1997. These nearshore and beach survey data were used to update the NOS database for contemporary nearshore and shoreline changes that have occurred following the most recent NOS surveys. Maps of the bathymetry in the near and farfield of the AES outfall are found in Figures 1.1 and 1.3 respectively.

To perform both the required wave shoaling and transport computations in the farfield of the infall and outfall, a relatively coarse-scale resolution of the bottom bathymetry is required which gives at least two grid points per wavelength of the highest frequency wave to be shoaled. The farfield grid to compute the effects of distant sources of storm water and pollution reaching the infall (Figure 1.3). A nearfield grid is nested inside the farfield grid and is used to calculate recirculated flow between the outfall and infall (Figure 1.1).

#### **D) Wave Climate**

Waves are the principle driving mechanism of mixing and current ventilation in the very nearshore region off Huntington Beach. This wave dominated region consists primarily of the surfzone but extends seaward into the wave shoaling zone a few surf zone widths beyond the point of wave breaking. Waves are also the most difficult of the 7 controlling variables to get long unbroken records. The availability of wave data in the lower Southern California Bight is what limited the period of record for this long term model analysis to 1980 - July 2000. Waves have been routinely monitored at several locations in the lower Southern California Bight since 1980 by the Coastal Data Information Program, (CDIP, 2004).

In the eastern North Pacific Ocean (where storms and swells effecting California are spawned) the La Niña condition leads to surface pressure

distributions and upper level wind systems that cause frontal cyclones from the Gulf of Alaska to follow storm tracks into the Pacific northwest (Figure 3.5a). During El Niño, surface pressures over the eastern North Pacific decline while jet stream flow develops extreme southward meanders, steering ocean storms into the Southern California Bight (Figure 3.5b).

Along the southern California coast a period of mild-stable weather occurred during the 30 years between the mid-1940's and mid-1970's when La Niña dominated storm systems like Figure 3.5a, (Inman and Jenkins, 1997) prevailed. Winters were moderate with low rainfall, and winds were predominantly from the west-northwest. The principal wave energy was from Aleutian lows having storm tracks which usually did not reach southern California (Figure 3.5a). Summers were mild and dry with the largest summer swells coming from very distant southern hemisphere storms.

The wave climate in southern California changed, beginning with the El Niño years of 1978-79 and extending at least until the present. The prevailing northwesterly winter waves were replaced by high energy waves approaching from the west or southwest (Figure 3.5b), and the previous southern hemisphere swell waves of summer have been replaced by shorter period tropical storm waves during late summer months from the more immediate waters off Central America (Inman, et al., 1996).

Data of instrumented buoys and light vessels in the North Pacific show that wave heights have increased significantly and continuously during the past 25 years. The measurements of six buoys between latitude 34°N and 56°N in the

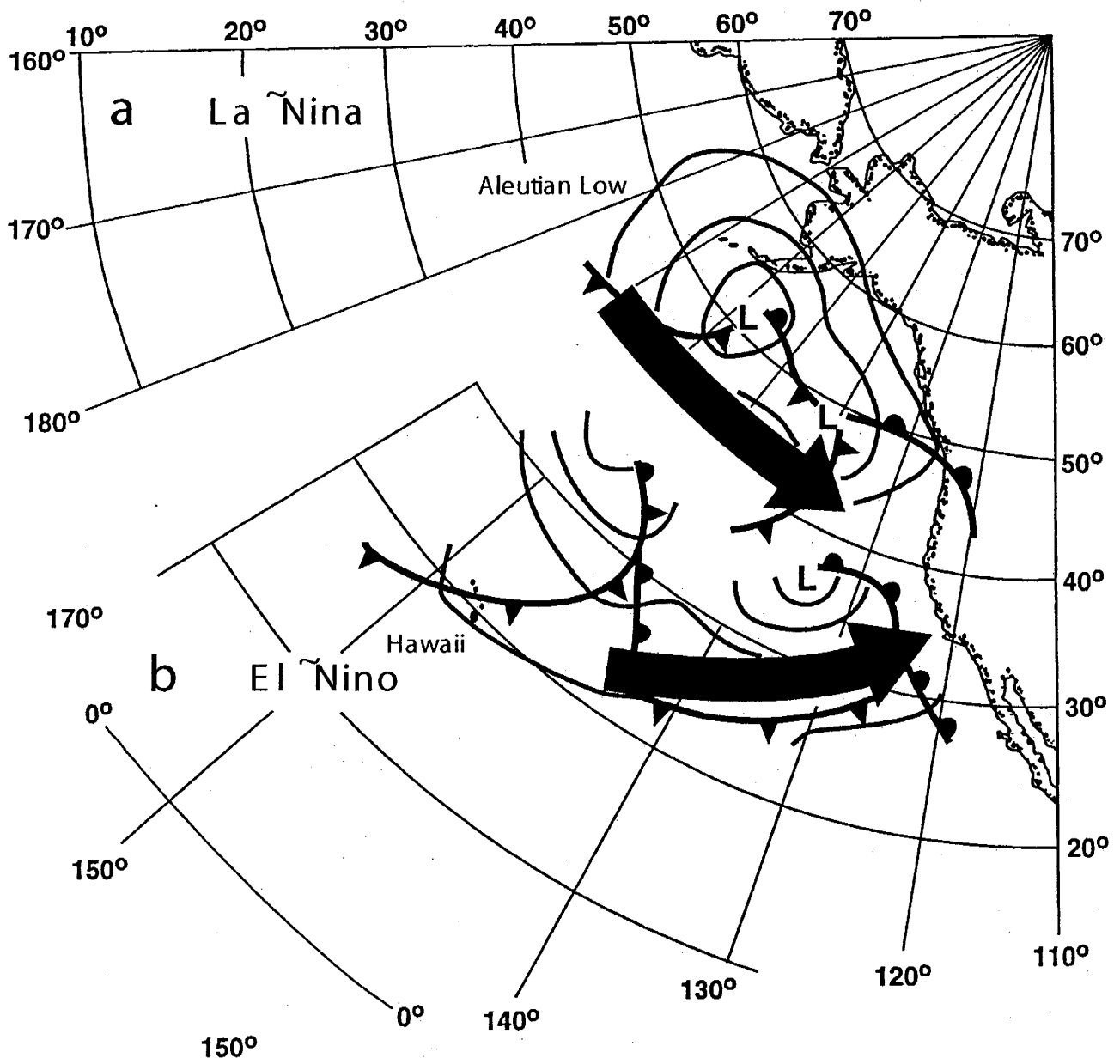


Figure 3.5. Typical storm track for a) La Niña and b) El Niño winter seasons.

eastern North Pacific cover the 25 year time interval from 1975-1999 (Allen and Komar, 2000). Over this period, the average annual (root-mean square) wave height increased progressively from about 1.6 m. to 1.9 m, generating a landward wave energy flux that ranged for these average waves from about  $93 \times 10^6$  kW to  $131 \times 10^6$  kW over the same period (Inman and Jenkins, 2000). This is highly significant because the transport rates and direction in the nearshore are directly proportional to the wave energy flux. To account for this recent trend, the model results of this study are based on the contemporary wave climate record of 1980-99.

El Niño storms generate two distinct swell patterns. These storms typically have an intense low pressure cyclone with an associated cold front, Figure 3.6. The storms that brought the extreme floods in February 1998 were El Niño storms. They are distinctive from the frontal cyclones occurring during La Niñas in that the cyclone portion of the storm tracks to much lower latitudes, (Figure 3.5b), and the associated cold front is very long, extending well into subtropical latitudes and entraining sub-tropical moisture. Consequently the pre-frontal winds which blow along the leading edge of the cold front have a very long fetch, while the warm subtropical moisture intensifies these winds through cyclogenesis. The intense, long fetch of the pre-frontal side of an El Niño storms gives rise to very high energy swells from the south-southwest. On the cold post frontal side of an El Niño storm, the winds blow from the west-northwest, but decrease rapidly with distance away from the cyclone (labeled L in Figure 3.6). Consequently the post frontal winds have a much shorter effective fetch and the post frontal north-northwesterly swells are less intense than the pre-frontal south-southwesterly swells. On the other hand the propagation of these storms is retarded when they

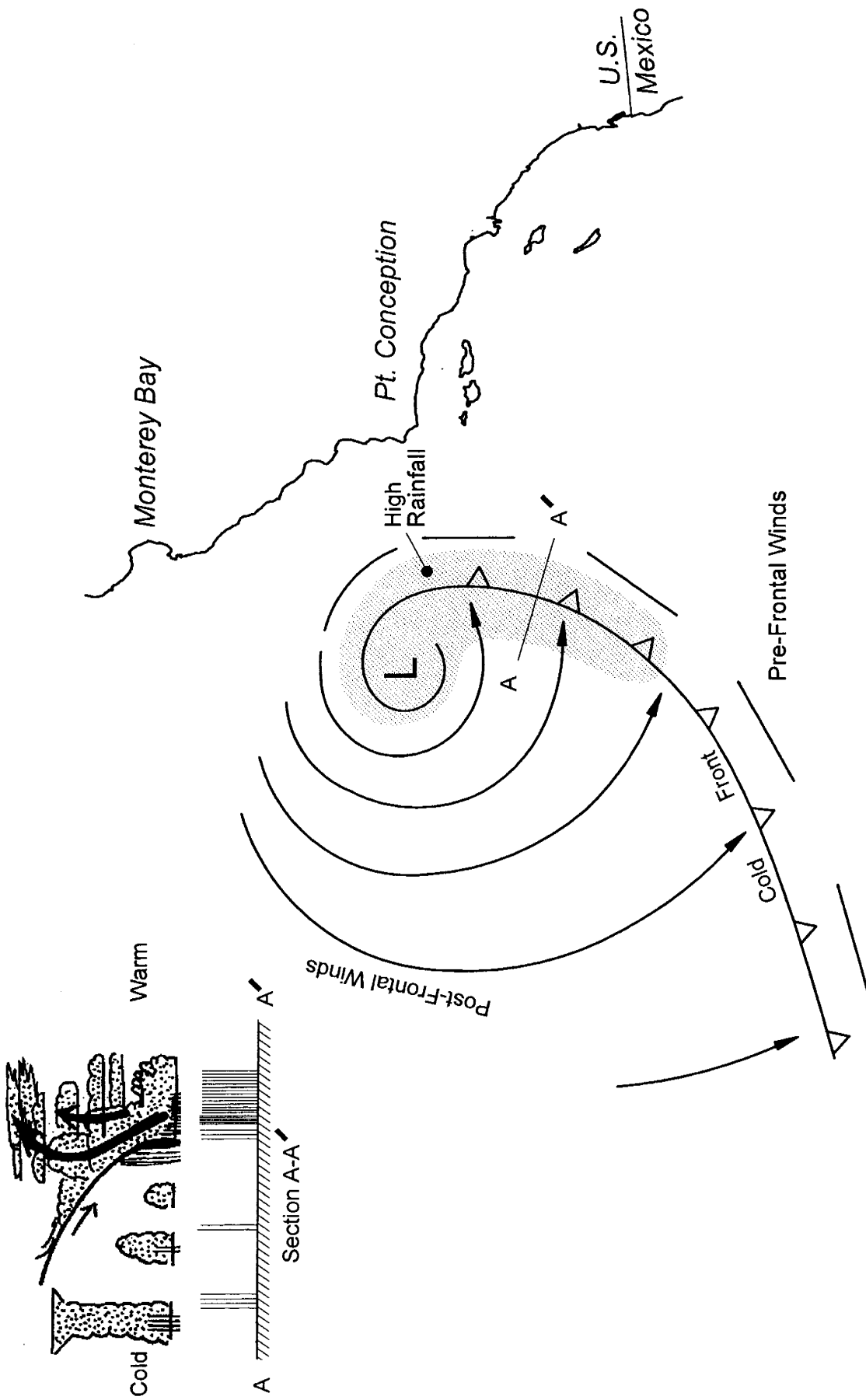


Figure 3.6. Anatomy of El Niño storms.

encounter the orography of the Southern California Bight, and thus the post-frontal swells are often more persistent and longer lived. In total, the El Niño storms have two distinct swell patterns that are directionally bipolar with regard to littoral drift along the lower reaches of the Bight. These directional characteristics tend to diminish the typical southward directed littoral drift, and instead act to drive the littoral drift back and forth along the coast with a small net direction.

In considering the predominant wave directions for high energy swells reaching the Huntington Beach area, the sheltering effects of the Channel Island System must be taken into account. Figure 3.7 shows that only certain gaps or “*wave windows*” between the islands and intervening land masses will allow the high energy, long period swells of distant storms to reach Huntington Beach. There are two distinct wave windows: 1) a *south window* providing wave exposure to swells approaching from between 160° and 200° true; 2) a *west window* open to swells from 255° to 279°. All remaining directions between these wave windows are open only to locally generated wind waves that are not likely to effect mixing and dilution below the thermocline.

For calibration and simulations of dispersion and dilution at AES Huntington Beach continuous unbroken wave records are required and must provide wave height, period and direction. Waves have been routinely monitored at several locations in the lower Southern California Bight since 1980 by the Coastal Data Information Program, (CDIP, 2004). The nearest CDIP directional wave monitoring sites are:

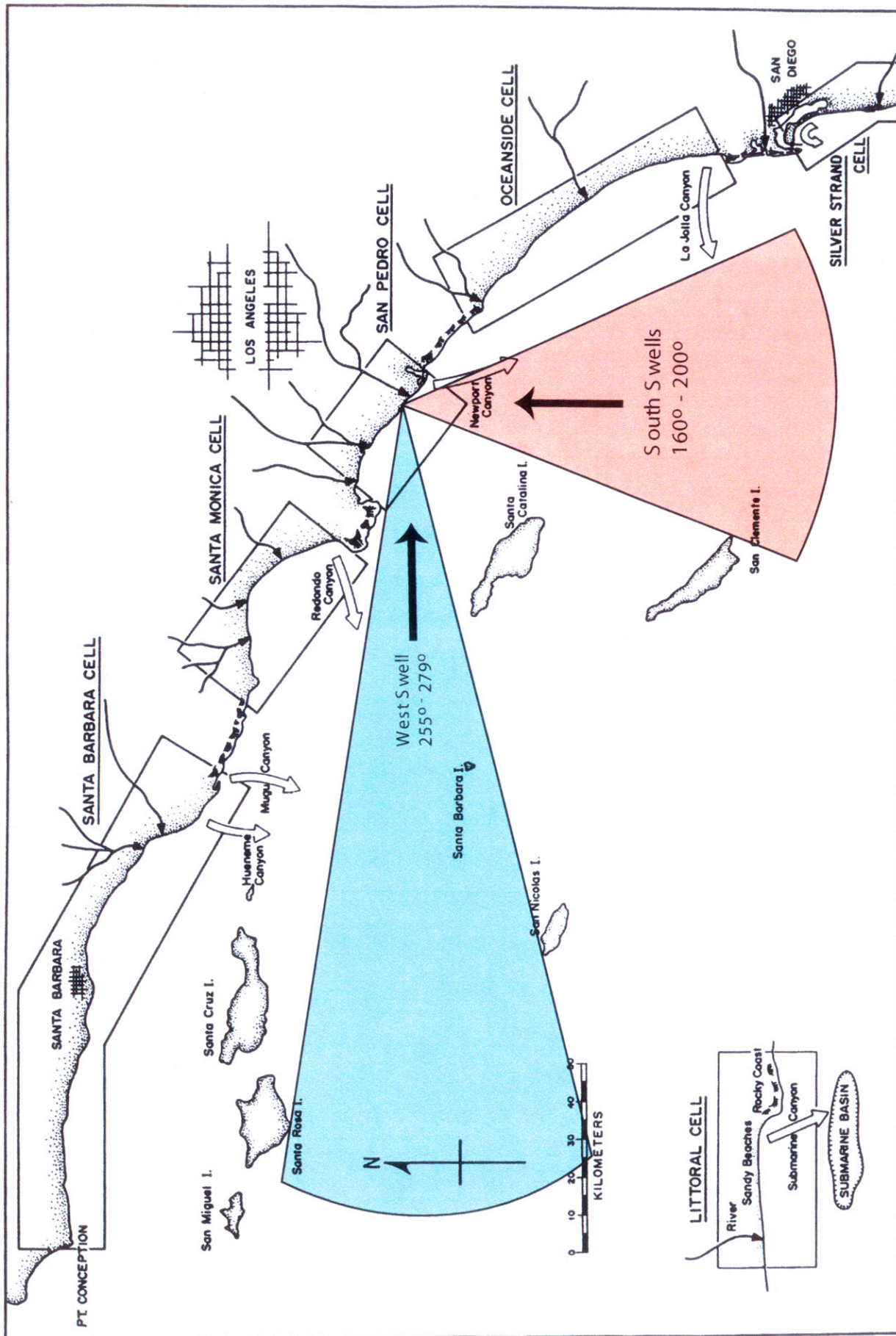


Figure 3.7. Island Sheltering Effects at AES Huntington Beach, CA Power Plant.

- a) **Huntington Beach Array**
- Station ID: 07201
  - Location:
    - 33 37.9'North, 117 58.7'West
    - Approximately 1 mile west of lifeguard headquarters at Huntington Beach, CA
  - Water Depth (m): 10
  - Instrument Description:
    - Underwater Directional Array
  - Measured Parameters:
    - Wave Energy
    - Wave Period
    - Wave Direction
- b) **San Clemente**
- Station ID: 05201
  - Location:
    - 33 25.2'North, 117 37.8'West
    - 1000 ft NW of San Clemente Pier
  - Water Depth (m): 10
  - Instrument Description:
    - Underwater Directional Array
  - Measured Parameters:
    - Wave Energy
    - Wave Period
    - Wave Direction
- c) **Oceanside Array**
- Station ID: 00401
  - Location:
    - 33 11.4'North, 117 23.4'West
    - 500 feet SW of pier
  - Water Depth (m): 10
  - Instrument Description:
    - Underwater Directional Array
  - Measured Parameters:
    - Wave Energy
    - Wave Period
    - Wave Direction

In addition to these CDIP sites waves have been monitored at Torrey Pines Beach from 1972 until 1984 by the SAS Stations deployed by Scripps Institution of Oceanography, (SIO), Pawka (1982). These data sets possessed gaps at various times due to system failure and a variety of start ups and shut downs due to program funding and maintenance. The undivided data sets were pieced together into a continuous record from 1980-2000 and entered into a structured preliminary data file. The data in the preliminary file represent partially shoaled wave data specific to the local bathymetry around each monitoring site. To correct these data to the nearshore of Huntington Beach, they are entered into a refraction/diffraction numerical code, back-refracted out into deep water to correct for local refraction and island sheltering, and subsequently forward refracted into the immediate neighborhood of Huntington Beach. Hence, wave data off each monitoring site was used to hindcast the waves at Huntington Beach.

The backward and forward refractions of CDIP and SIO data to correct it to Huntington Beach was done using the numerical refraction-diffraction computer code, **OCEANRDS**. The primitive equations for this code are lengthy, so a listing of the FORTRAN codes of **OCEANRDS** appear in Appendix D. These codes calculate the simultaneous refraction and diffraction patterns propagating over a Cartesian depth grid. A large outer grid was used in the back refraction calculations to correct for island sheltering effects, while a high resolution inner grid was used for the forward refraction over the complex bathymetry around Huntington Beach and the OCSD deep outfall. **OCEANRDS** uses the parabolic equation method (PEM), Radder (1979), applied to the mild-slope equation, Berkhoff (1972). To account for very wide-angle refraction and diffraction relative to the principle wave direction, **OCEANRDS** also incorporates the high order PEM Pade approximate

corrections modified from those developed by Kirby (1986a-c). Unlike the recently developed REF/DIF model due to Dalrymple, et al. (1984), the Pade approximates in “OCEANRDS” are written in tesseral harmonics, per Jenkins and Inman (1985); in some instances improving resolution of diffraction patterns associated with steep, highly variable bathymetry such as found near the Newport Submarine Canyon. These refinements allow calculation of the evolution and propagation of directional modes from a single incident wave direction; which is a distinct advantage over the more conventional directionally integrated ray methods which are prone to caustics (crossing wave rays) and other singularities in the solution domain where bathymetry varies rapidly over several wavelengths.

An example of a reconstruction of the wave field throughout the Bight is shown in Figure 3.8 using the back refraction calculation of the CDIP data from the San Clemente array. Wave heights are contoured in meters according to the color bar scale and represent 6 hour averages, not an instantaneous snapshot of the sea surface elevation. Note how the sheltering effects of Catalina and San Clemente Islands have induced longshore variations in wave height throughout the Southern California Bight. Figure 3.9 shows the deep water significant wave heights, periods and directions resulting from the series of back-refraction calculations for the complete CDIP and SIO data set at  $\Delta t = 6$  hour intervals over the 1980-2000 period of record. The data in Figure 3.9 are the values used as the deep water boundary conditions on the farfield grid (Figure 1.3) for the forward refraction computations into the Huntington Beach region. The deep water wave angles are plotted with respect to the direction (relative to true north) from which

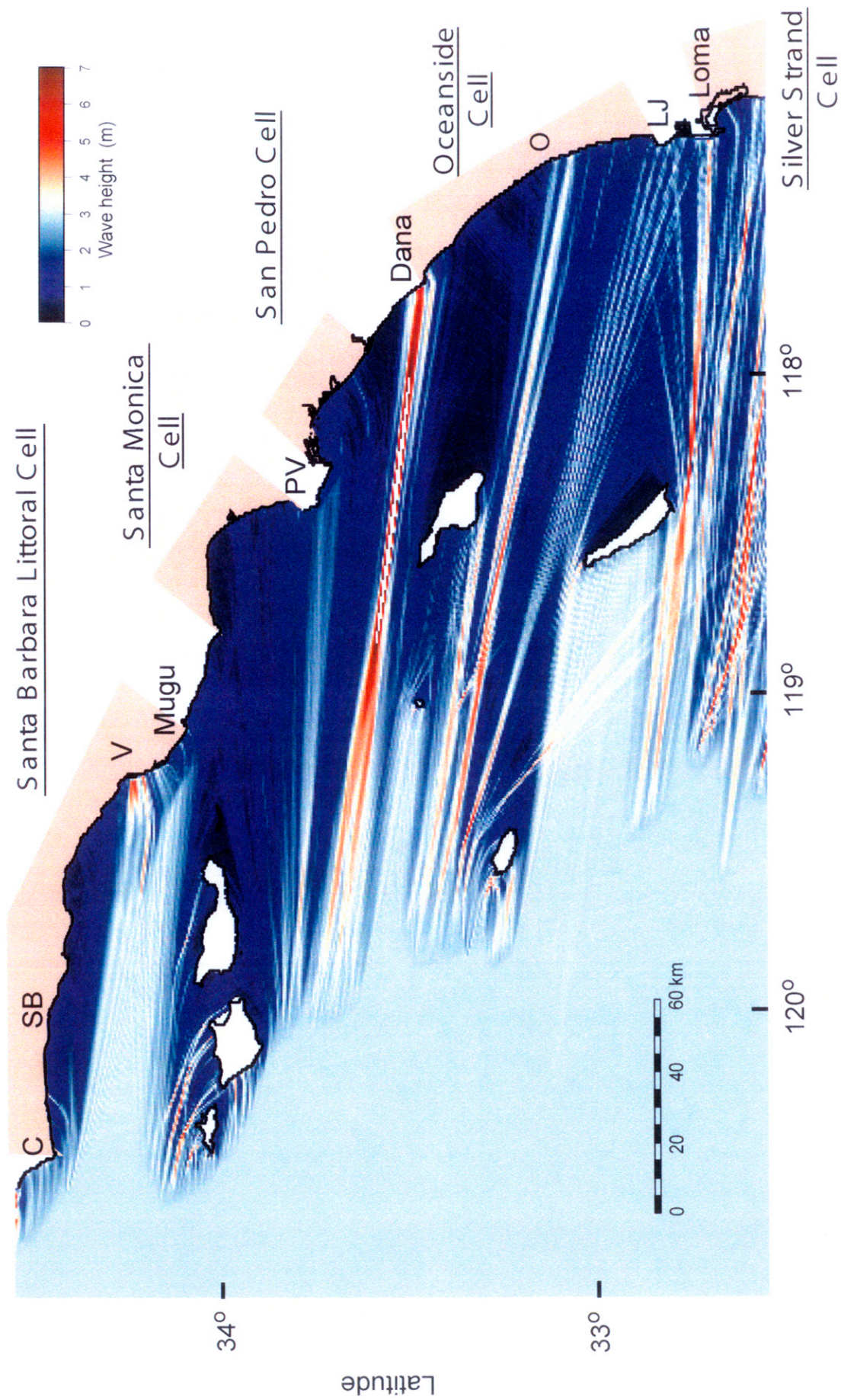
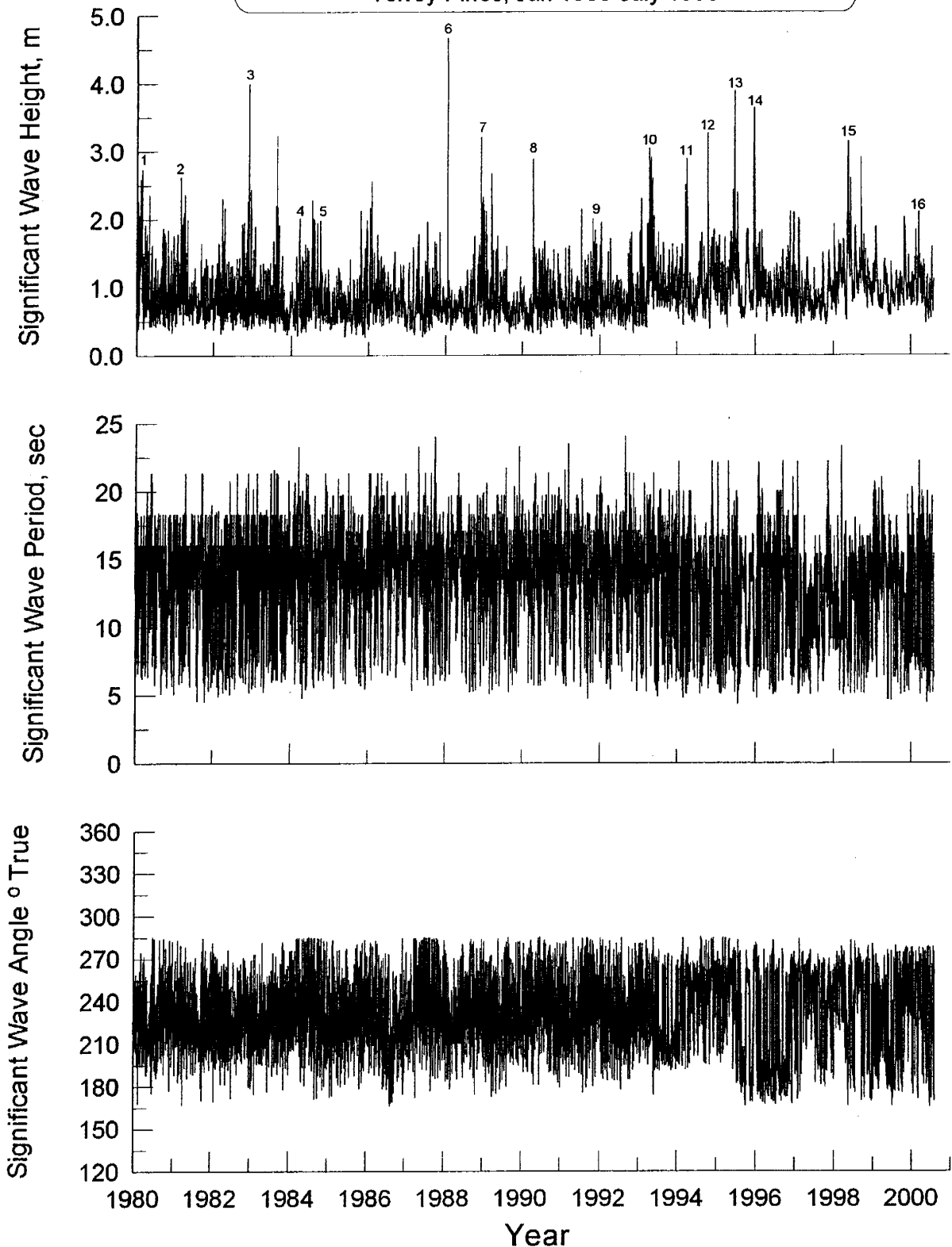


Figure 3.8. Back refraction of San Clemente CDIP data, for 13 January 1993 storm with 3 m high 15 sec waves approaching the Southern California Bight from 285°, an example of a moderate El Niño storm.

the waves are propagating at the deep water boundary of the farfield grid (Figure 1.3). Inspection of Figure 3.9 reveals that a number of large swells lined up with the wave windows open to Huntington Beach during the El Niño's of 1980-83, 1986-88, 1992-95, and 1997-98. The largest of these swell events was the 18 January 1988 storm, producing 4.5 m deep water swells off Huntington Beach (see event #6 in Figure 3.9).

Figure 3.10 gives an example of the forward refraction calculation over the farfield grid of the Huntington Beach region for the largest swells occurring during the peak flow month of February 1998. These swells occurring 5 February 1998 not concurrent with the peak flow event in the Santa Ana River which occurred later in the month on 24 February 1998. The 5 February 1998 swells were pre-frontal southwesterly for-runners of the El Niño storm that struck the Huntington Beach region with a series of powerful squalls between 7 and 10 February 1998. This was the second largest flood event of February 1998. The highest rainfall producing storm of the month was accompanied by southwesterly swells that were almost as large as the 5 February 1998 fore-runners. These swells arrived concurrent with the peak rainfall event of 24 February 1998 El Niño storm and produced the regional refraction pattern shown in Figure 3.11. Comparing the refraction patterns of both storms in Figures 3.10 and 3.11, we find a region of intensified wave heights at the AES infall. This is referred to as a *bright spot* in the refraction pattern and represents an area where wave energy has been focused, (in this case by the refraction caused by a small canyon in the shelf directly offshore of AES Huntington Beach). The increased wave heights in the bright spot at the infall increase the mixing and turbulence generated by the seabed

Data Reconstructed From CDIP and SIO Arrays:  
 Oceanside, July 1983-Oct 1991 & May 1998-May 2000  
 San Clemente, Aug 1991-Jun 1993 & Sep 1993-Apr 1998  
 Huntington Beach, July 1993-Aug 1993  
 Torrey Pines, Jan 1980-July 1983



**Figure 3.9.** Deep water wave data for dispersion and dilution analysis at AES Huntington Beach, CA.

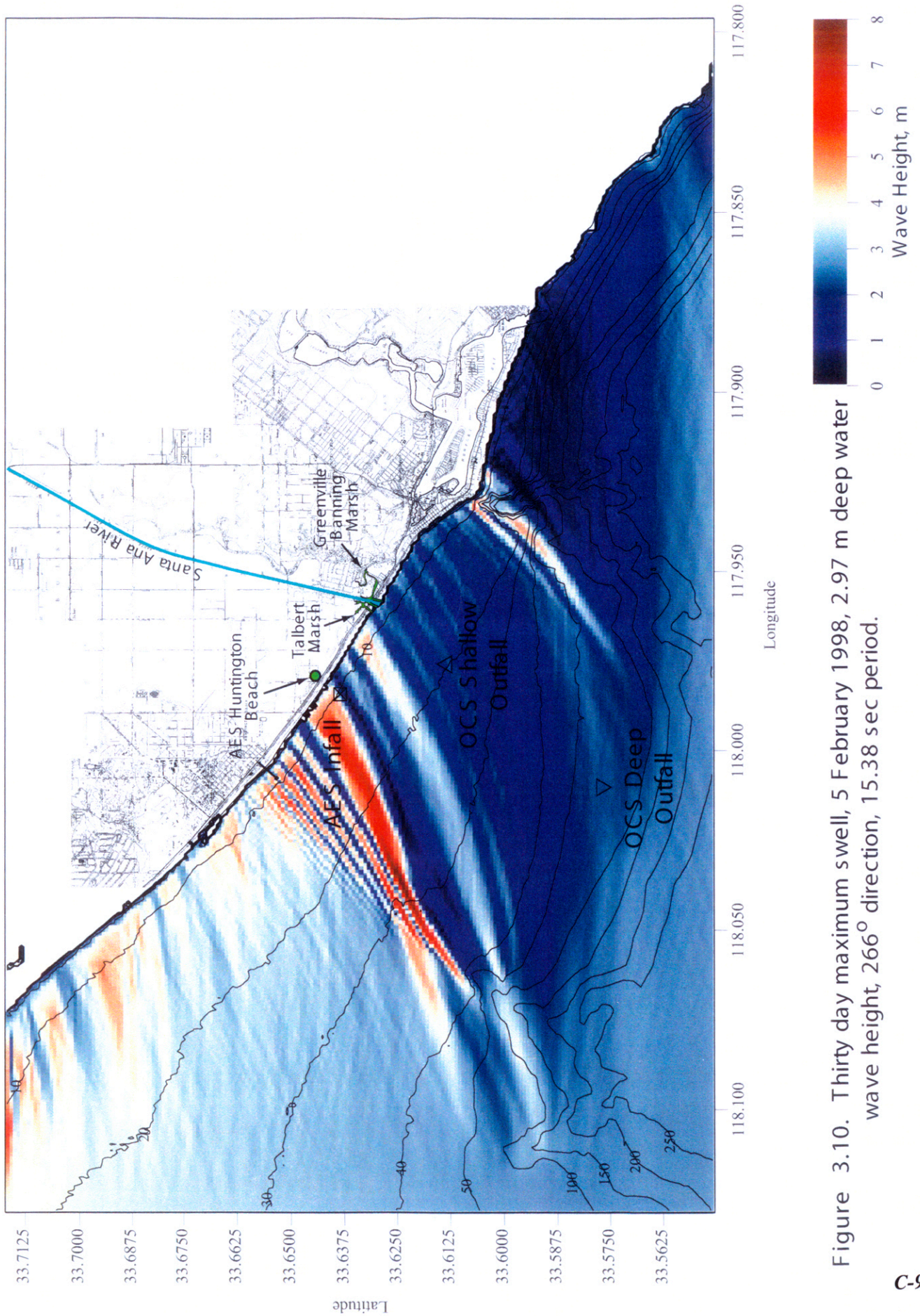


Figure 3.10. Thirty day maximum swell, 5 February 1998, 2.97 m deep water wave height, 266° direction, 15.38 sec period.

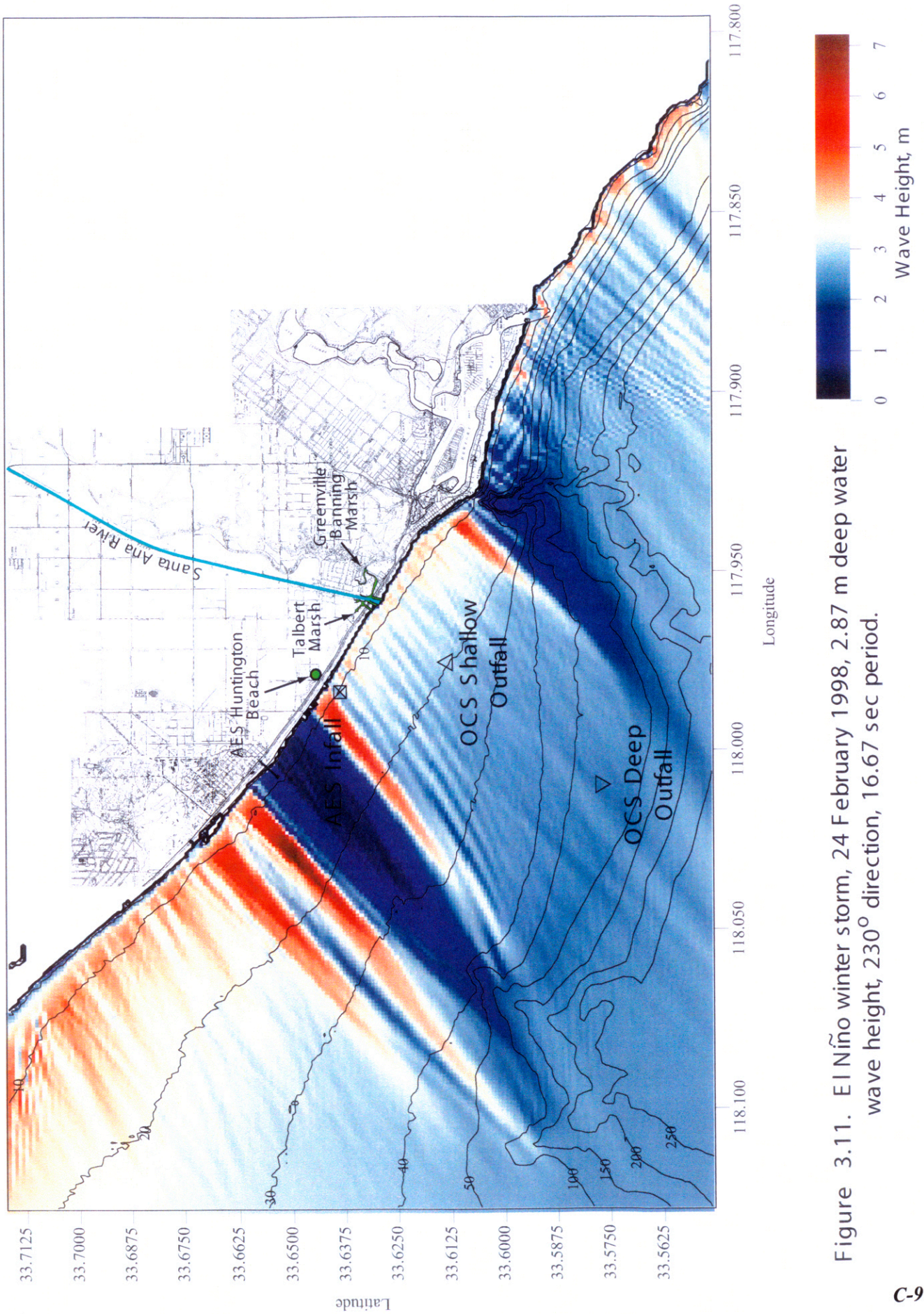
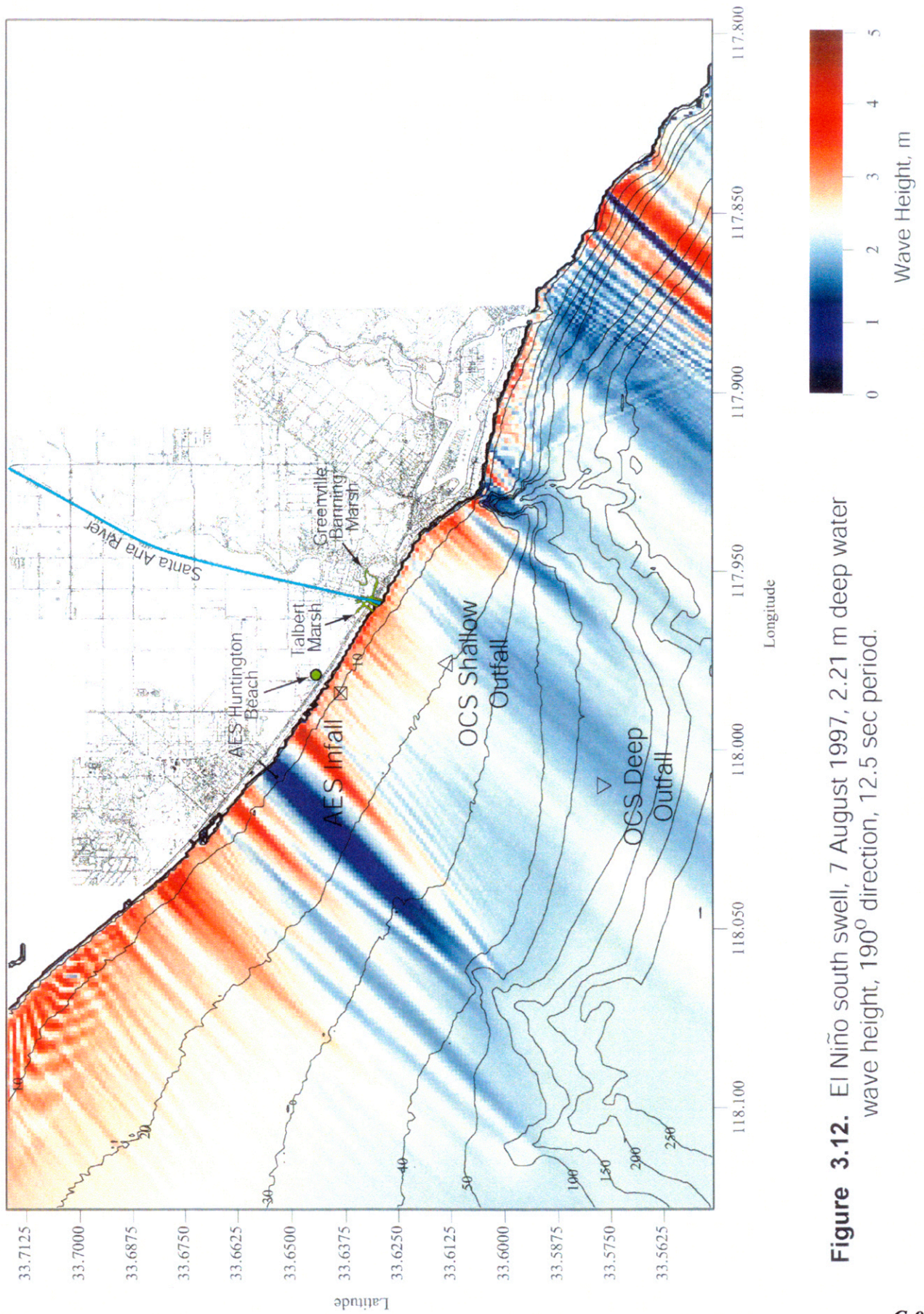


Figure 3.11. El Niño winter storm, 24 February 1998, 2.87 m deep water wave height, 230° direction, 16.67 sec period.

boundary layer and by oscillatory wakes of the infall tower structure. This increases the likelihood of the heavier than seawater by-products of the RO process being mixed upward into the water column from the discharge and subsequently recirculated through the infall. Therefore these El Niño winter storm waves serve to provide low flow case scenarios for evaluating re-circulation effects on source water make-up (Sections 7-9).

To evaluate maximum likelihood scenarios for the northward transport of bacteria from Talbert Marsh or the wastefield from the OCSD deep outfall toward the AES infall, we consider summer time El Niño wave conditions like those that occurred 7 August 1997, Figure 3.12. The extreme southerly direction of these waves (from 190°) produce northward flowing wave induced mass transport in shallow water. Inspection of Figure 3.12 shows a fairly uniform shoaling of incident waves between the Santa Ana River and the AES infall. We also find that the bright spot of intensified wave mixing has moved north of the AES infall. This shift in the bright spot does not diminish the low flow case pessimism because the OCSD wastefield is buoyant and does not require intense local mixing to raise it in the water column to the elevation of the infall velocity cap.

Refraction patterns for other storms evaluated from the period of record for effects on source water and dilution are contained in Appendix G. In addition to these, Appendix G contains the refraction of the 30 day average minimum wave and the average annual wave. The 20.5 year record of daily mean wave height is plotted in Panel-b of Figure 3.24 found at the end of this section, summarizing the complete set forcing functions.



**Figure 3.12.** El Niño south swell, 7 August 1997, 2.21 m deep water wave height, 190° direction, 12.5 sec period.

### **E) Current Forcing**

While waves dominate the initial dilution and dispersion of heat and concentrated seawater discharge in the inshore domain, the tidal currents control dilution and dispersion in the offshore domain, particularly in the immediate neighborhood of the AES outfall. Tidal currents were calculated using the tidal constituents from the tide gage station at Los Angeles (NOAA #941-0660). Current forcing is predominantly tidal in the offshore domain of the Huntington Beach coastal region in Figure 1.3, and is a combination of tidal and wave-induced currents in the nearshore domain.

Tidal currents are mixed semi-diurnal with both progressive and standing components in the mid to inner shelf. Tidal currents flow parallel to the shore in a northwestward direction on flood tide (Figure 3.13) and southeastward on an ebb tide (Figure 3.14). The tidal current speed diminishes towards shore due to friction in the shallow coastal boundary layer, and the phase of the tidal motion varies in the cross-shore direction such that during tidal reversals from ebb to flood, the phase of the inshore motion is lagging the offshore motion (Figure 3.15). The maximum currents in the offshore domain are typically 40 to 70 cm/sec. Along the Huntington/Newport Beach coast the tidal currents are ebb dominated such that over one tidal day (24 hr 50 min) the net current flows downcoast to the southeast as shown in Figure 3.16 for the peak runoff event day of 24 February 1998. Each progressive vector plot in Figures 3.13 to 3.16 is composed of self-scaling vectors in units of cm/sec proportional to the vector length in the lower left hand corner, which represents the largest current vector found anywhere on the plot.

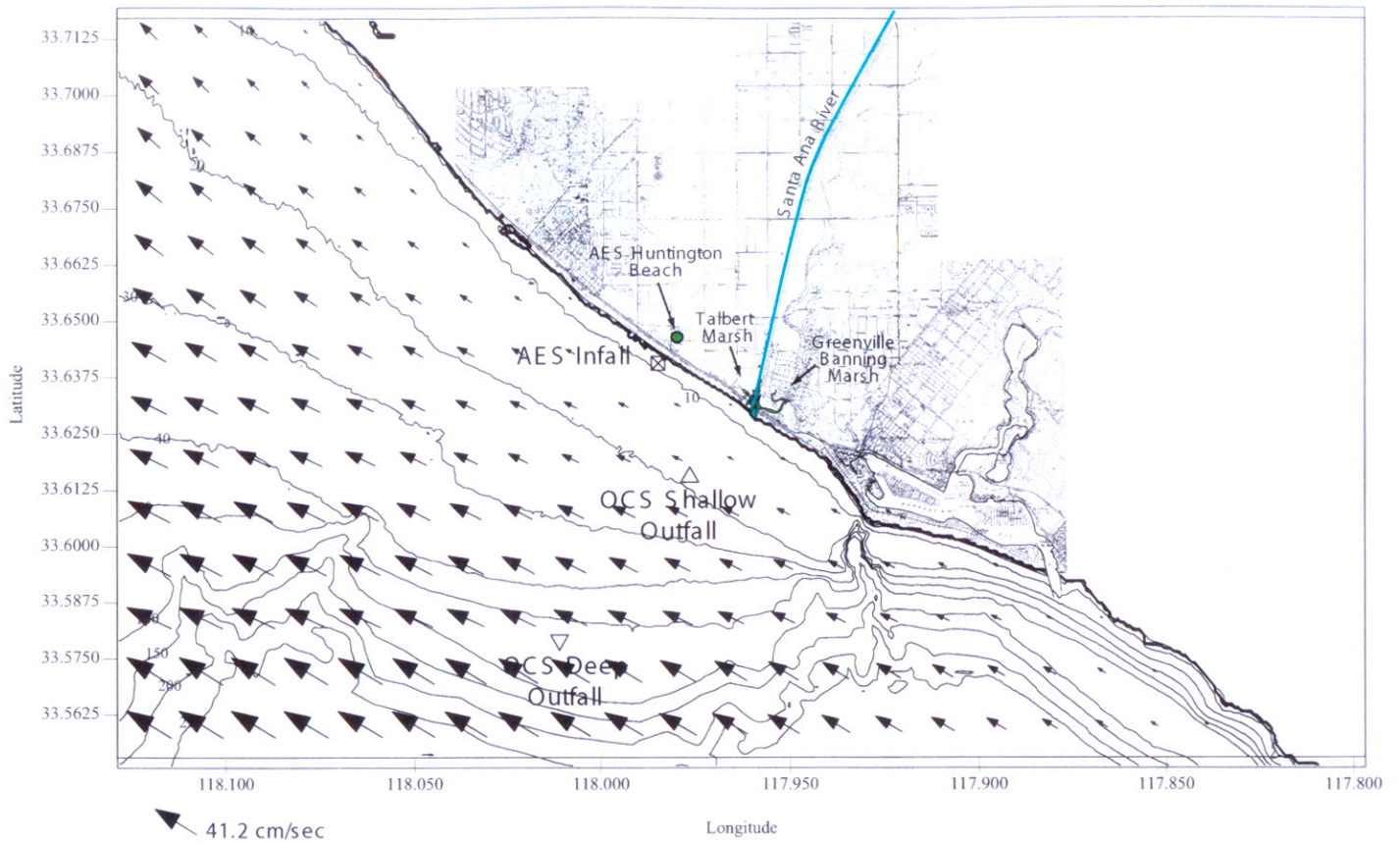


Figure 3.13. Tidal current simulation for Newport - Huntington Beach, flood tide, 24 February 1998, 04:09 PST. Current vector magnitude relative to largest vector arrow shown (41.2 cm/sec).

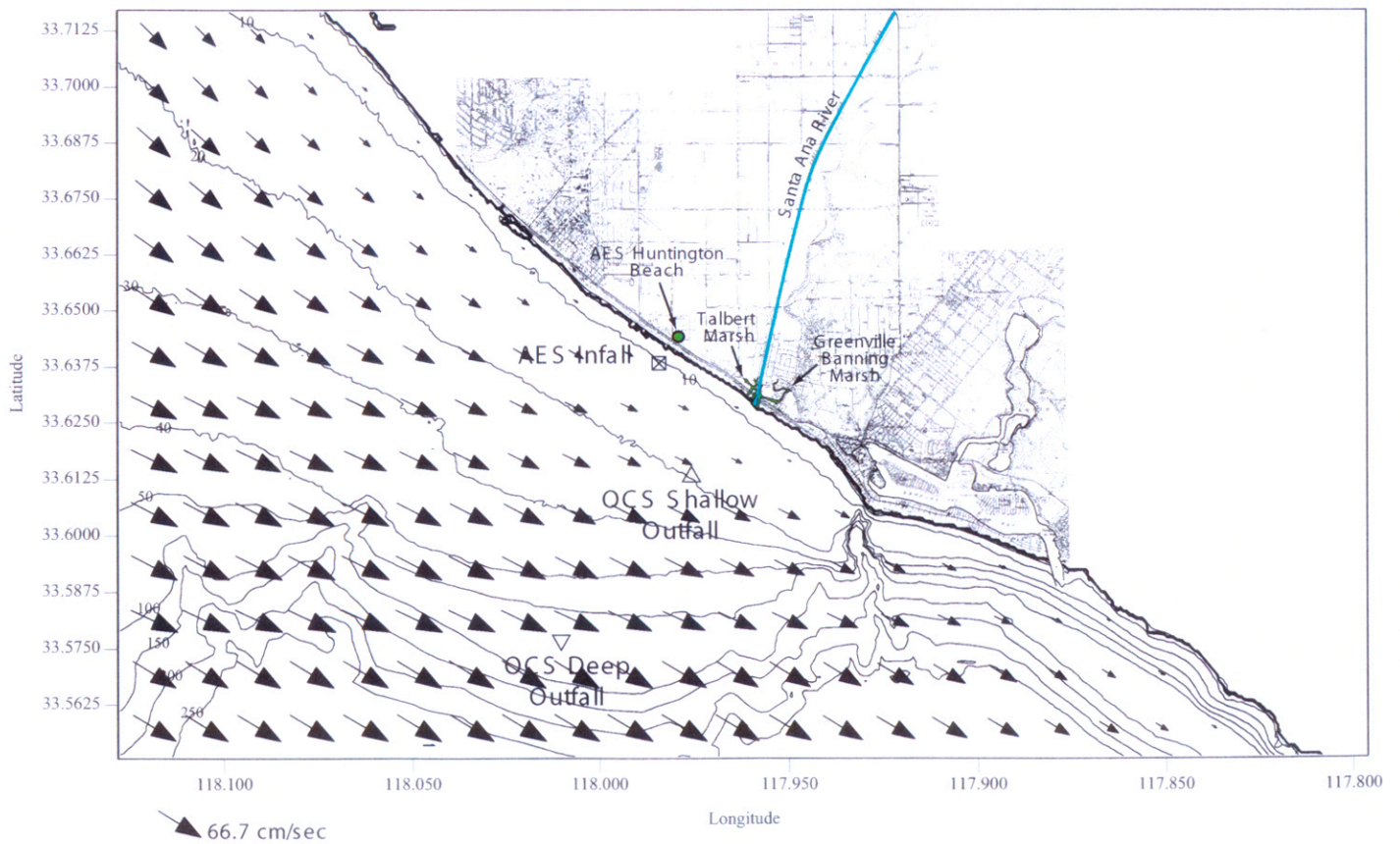


Figure 3.14. Tidal current simulation for Newport - Huntington Beach, ebb tide, 24 February 1998, 10:54 PST. Current vector magnitude relative to largest vector arrow shown (66.7 cm/sec).

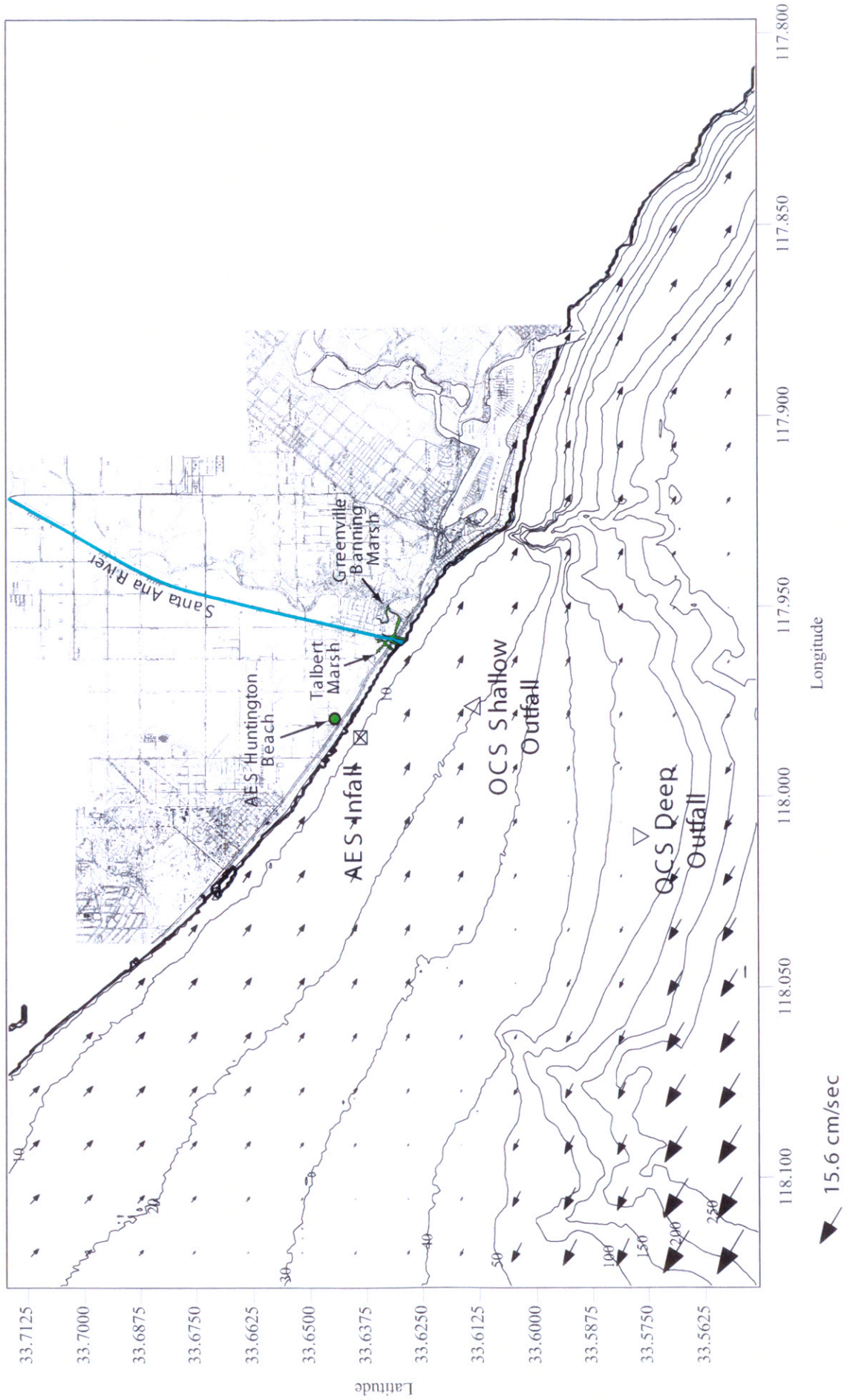


Figure 3.15. Tidal current simulation for Newport - Huntington Beach, ebb to flood tide transition, 24 February 1998, 14:10 PST. Current vector magnitude relative to largest vector shown (15.6 cm/sec).

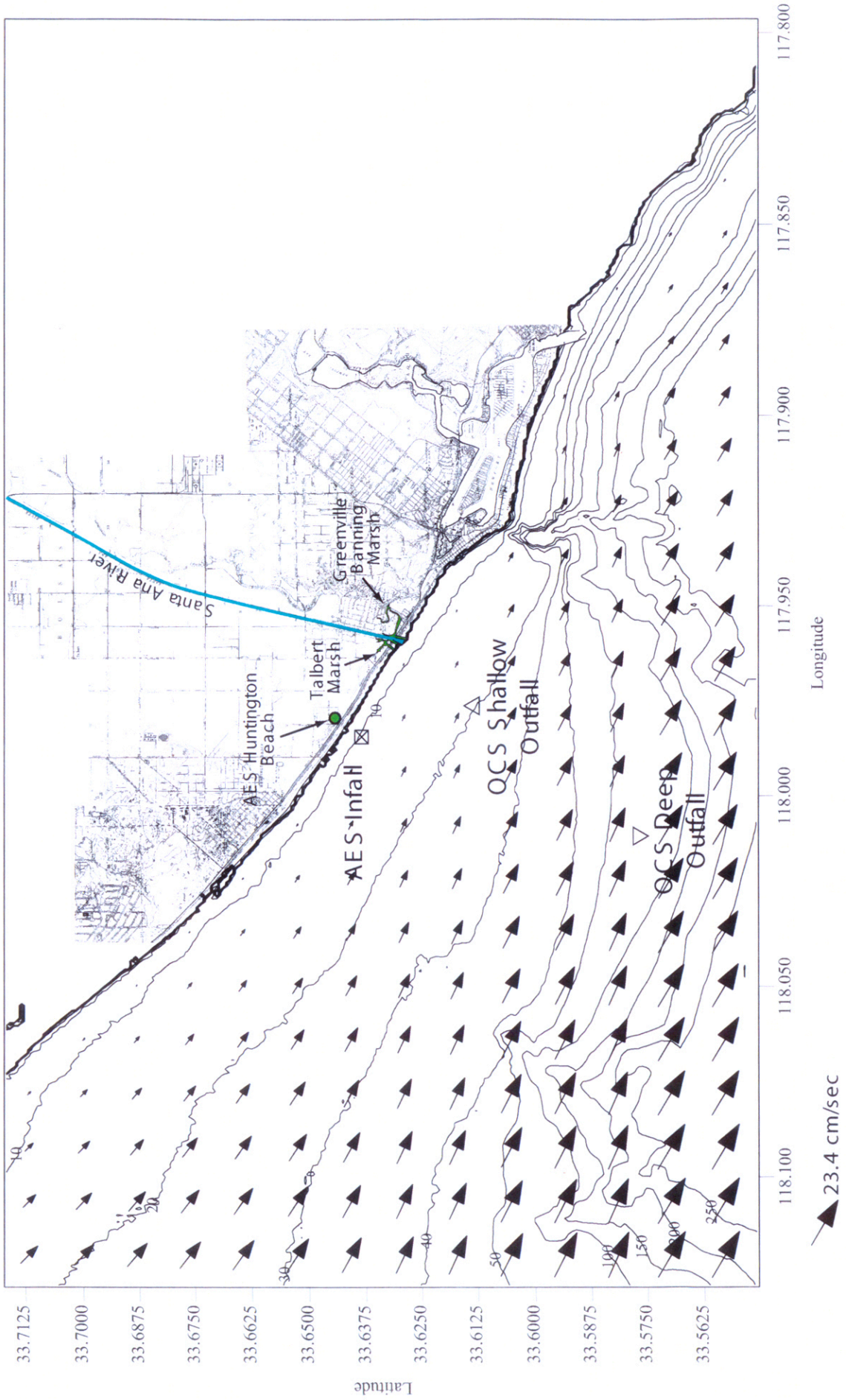


Figure 3.16. Tidal current simulation for Newport - Huntington Beach, tidal day, 24 February 1998. Current vector magnitude relative to largest vector arrow shown (23.4 cm/sec).

Wave induced currents predominate nearshore where wave shoaling effects are maximum. Wave induced currents increase with increasing wave height and remain significant over a nearshore domain extending 4 to 5 surf zone widths seaward of the shoreline. They flow longshore generally in the direction of longshore energy flux and away from areas of high waves (bright spots) and towards areas of low waves (shadows). These longshore currents increase with increasing wave height and obliquity. Figure 3.17 gives an example of the wave induced longshore currents for the El Niño storm of 24 February 1998. Note how these currents are confined to the very nearshore and how they are directionally controlled by the local refraction in Figure 3.11.

Figure 3.18 gives the progressive vector plot for the 7 day average of the combined tidal and wave-induced current field during the peak flow period of the Santa Ana River (Figure 3.2). We note that the net transport over a 7-day period is downcoast to the southeast due to the ebb dominance of the tidal currents. Inshore the net transport is very small because the wave and tidal currents tend to cancel out one another over a 7-day period. However over shorter periods of time for the summer El Niño conditions in August 1997 sustained large south swells cause a reversal in the net transport in the inshore domain (Figure 3.19). These inshore current structures will be overlaid on the spring flood tide condition on 17 August 1997 with sustained northerly transport throughout the middle and inner shelf domain (Figure 3.20). Together these 2 current fields (Figure 3.19 & Figure 20) produce a composite low flow case model scenario for evaluating the potential for dispersion of the OCSD wastefield into the neighborhood of the AES in-fall. The 20.5 year record of daily maximum tidal currents is plotted in Panel-b of Figure

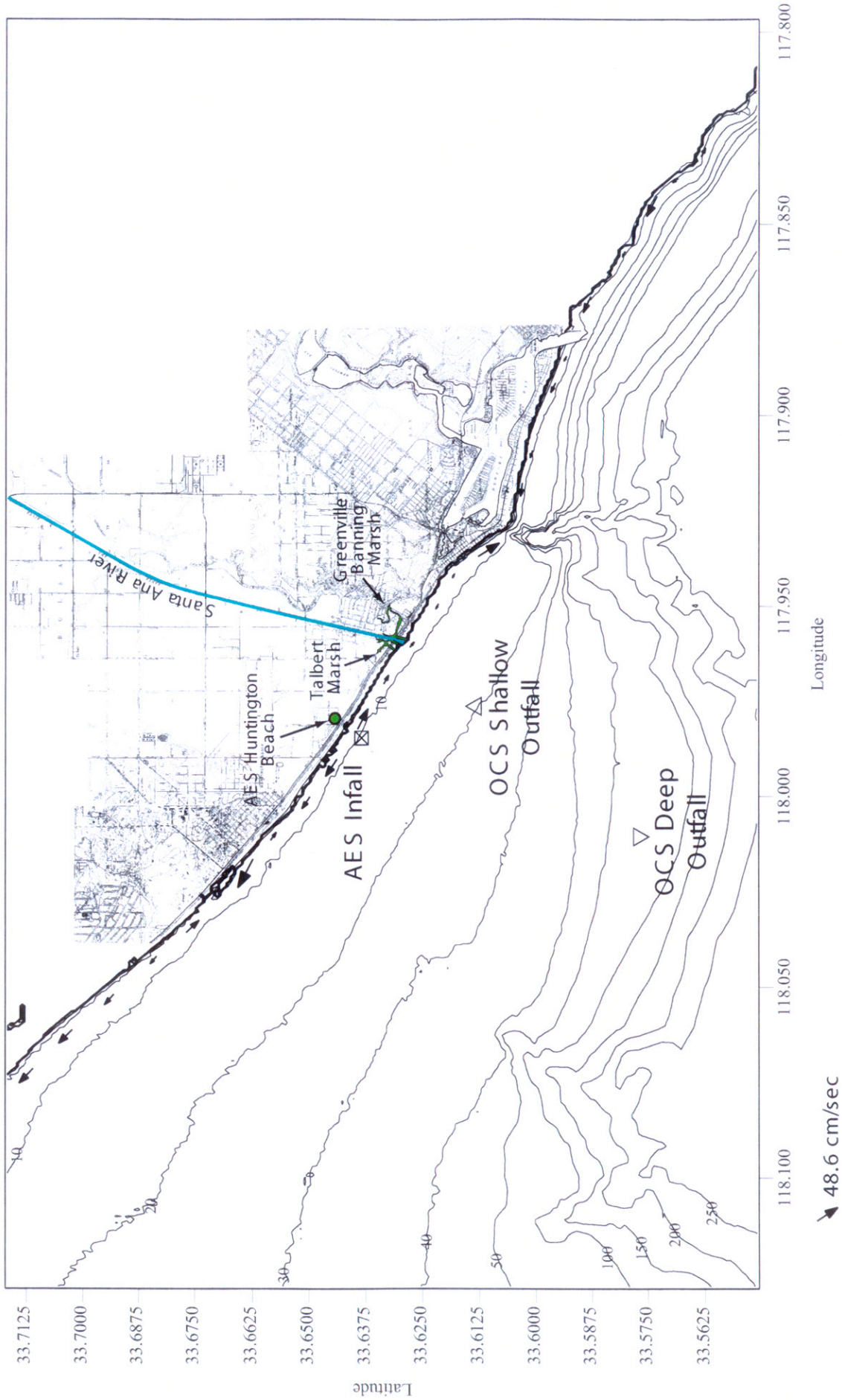


Figure 3.17. Wave current simulation for Newport - Huntington Beach, 24 hour average, 24 February 1998, 23:38 PST. Current vector magnitude relative to largest vector magnitude shown (48.6 cm/sec).

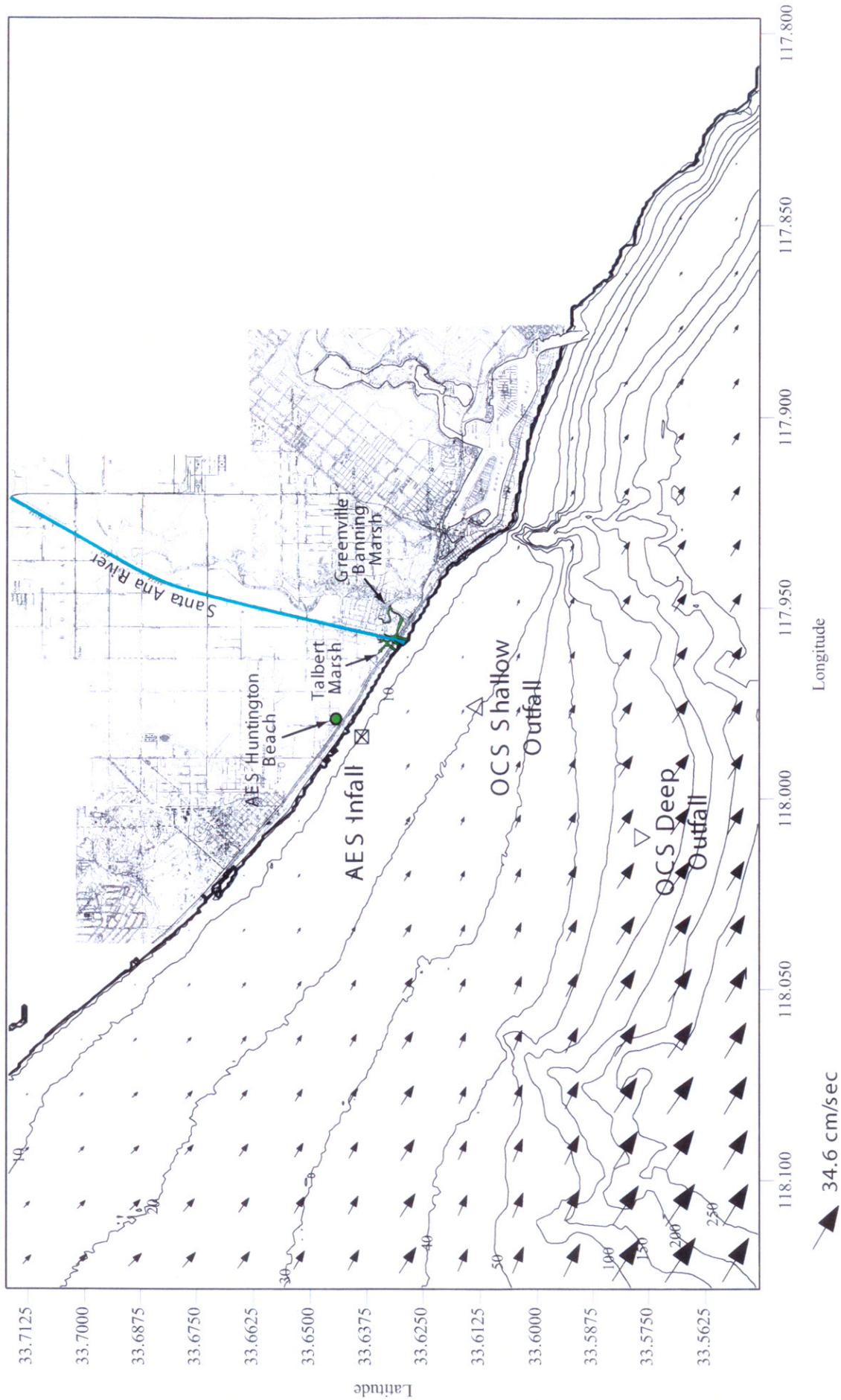


Figure 3.18. Mean current simulation ( 7 day average ) for Newport - Huntington Beach, 22-28 February 1998, Current vector magnitude relative to largest vector arrow shown (34.6 cm/sec).

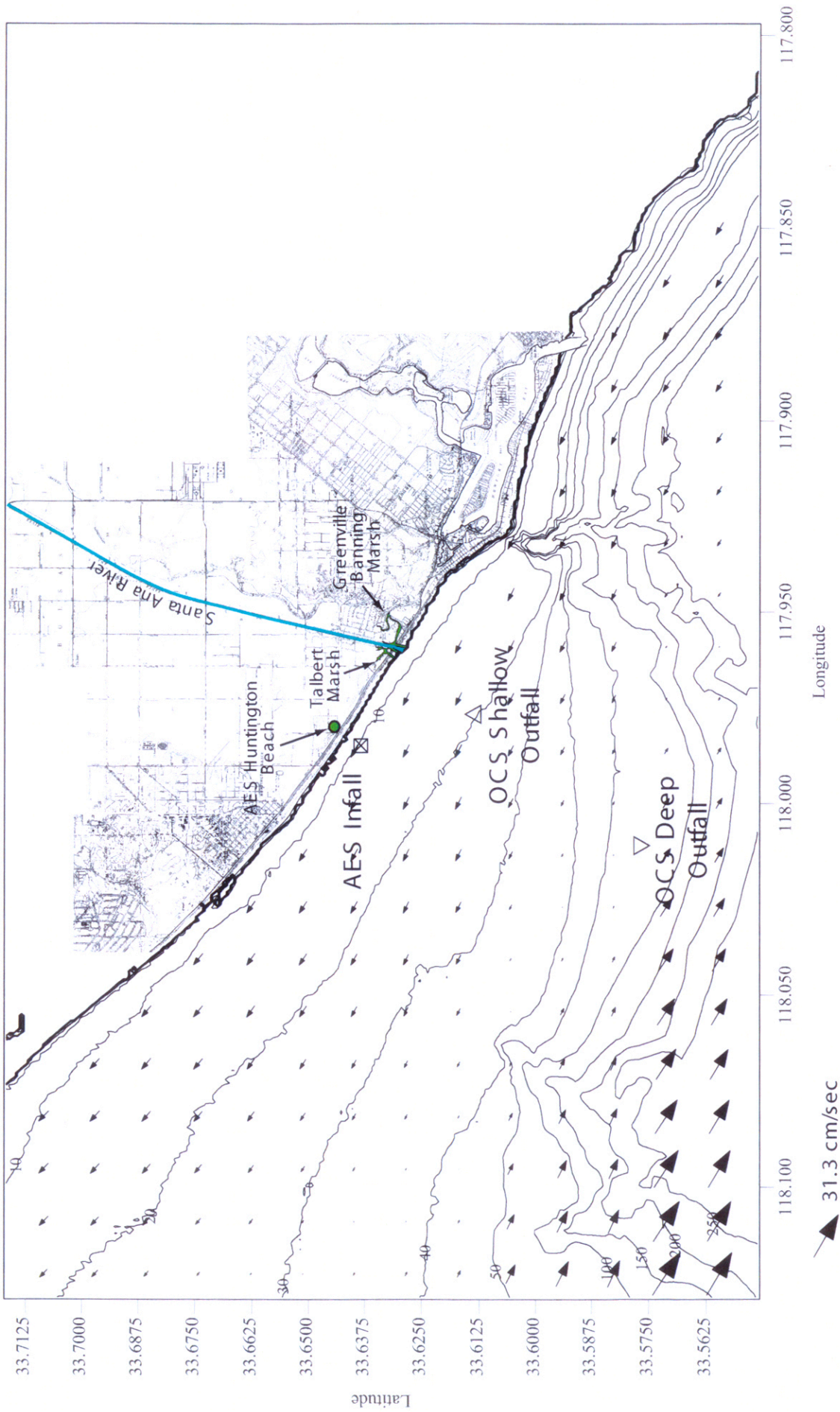


Figure 3.19. Mean current simulation ( 3 day average, El Niño ) for Newport - Huntington Beach, 7-10 August 1997, Current vector magnitude relative to largest vector arrow shown (31.3 cm/sec).

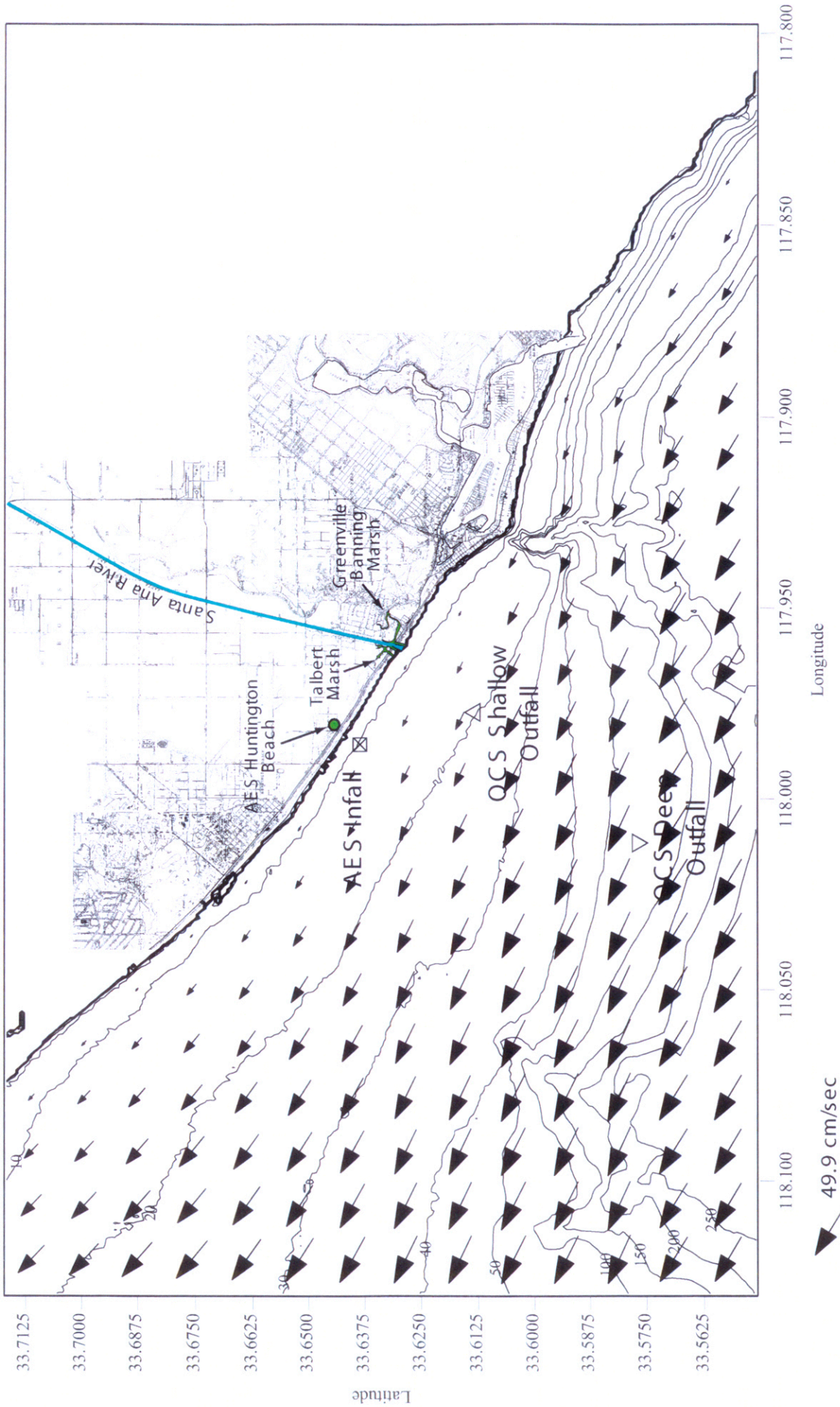


Figure 3.20. Current simulation for Newport - Huntington Beach, flood tide, 17 August 1997, 00:21 PST, Current vector magnitude relative to largest vector arrow shown (49.9 cm/sec).

3.24 found at the end of this section, summarizing the complete set forcing functions.

#### **F) Wind Mixing**

Winds provide considerable mixing in the surface layer off Huntington Beach Daily that typically extends down to depths of 10-20 m. Winds also provide wind drift which although weak can bridge the gap between the off shore tidally dominated regime and the inshore wave-dominated regime. The collection of historical wind data are compiled in US Surface Airways Data available from the National Climate Data Center document library (NCDC , 2004). The closest NCDC Surface Airways monitoring location relative to Huntington Beach is Long Beach Daugherty Field. Here, human observations of surface winds were collected and archived by NCDC beginning 1 January 1964 until 31 August 1996, after which wind observations were taken by means of the Automated Surface Observing System (ASOS). Combining these 2 data bases, a continuous surface wind record was assembled for the period 1980-2000 as shown in Panel-c of Figure 3.24, along with the other forcing functions summarized at the end of this section. Because the lower Southern California Bight is a “wind drought” region due to orographic blocking by the Penninsular Range, the 20.5 year mean wind speed is only 5.6 knots. However, El Niño storms and North Pacific cold fronts episodically increase wind speeds to a maximum 24 hour mean of 19.6 knots, as occurred during the 1997 El Niño storms. The minimum daily mean wind speed is 0 knots. The long term record in Figure 3.24 shows a well defined inter annual (seasonal) modulation of daily mean winds, with a 3-7 year intensification associated with El Niño.

### **G) Ocean Salinity**

Ocean salinity variation exerts a modulating effect on the concentration of sea salts discharged from the desalination plant. The proposed desalination plant will divert approximately 100 mgd of heated HBGS condenser seawater through a reverse osmosis system (RO) before in-plant waste streams are added to the cooling water discharge. The RO system will produce 50 mgd of product from the 100 mgd of cooling water diverted from the condenser cooling stream. The RO system will discharge 50 mgd of concentrated seawater by-product at twice ambient ocean salinity, which is subsequently diluted in the remaining cooling water discharge stream. Therefore, the concentration of sea salts in the discharge varies directly with ocean salinity at the intake to the generating station.

Figure 3.21a shows the variation in daily mean salinity in the coastal waters off Huntington Beach derived from 20.5 years of NPDES monitoring data of the AES and OCSD outfall for the period from 1980 until mid-2000. Gaps in these daily records were filled salinity monitoring data from the Scripps Pier Shore Station located 109 km (67.8 miles) to the south east of the AES outfall, (SIO, 2001). Inspection of Figure 3.21a indicates that the ocean salinity varies naturally by 10% between summer maximums and winter minimums, with a long term average value of 33.52 parts per thousand (ppt). Maximum salinity was 34.34 ppt during the 1998 summer El Nino when southerly winds transported high salinity water from southern Baja up into the Southern California Bight. Minimum salinity was about 31.02 ppt during the 1993 winter floods. The variation between maximum and minimum salinity is about 3.32 ppt, which is about 10% of the average value of 33.5 ppt. An ocean salinity histogram is given in Figure 3.21b that indicates the ocean salinity exceeded the 33.5 ppt average value during 2,488

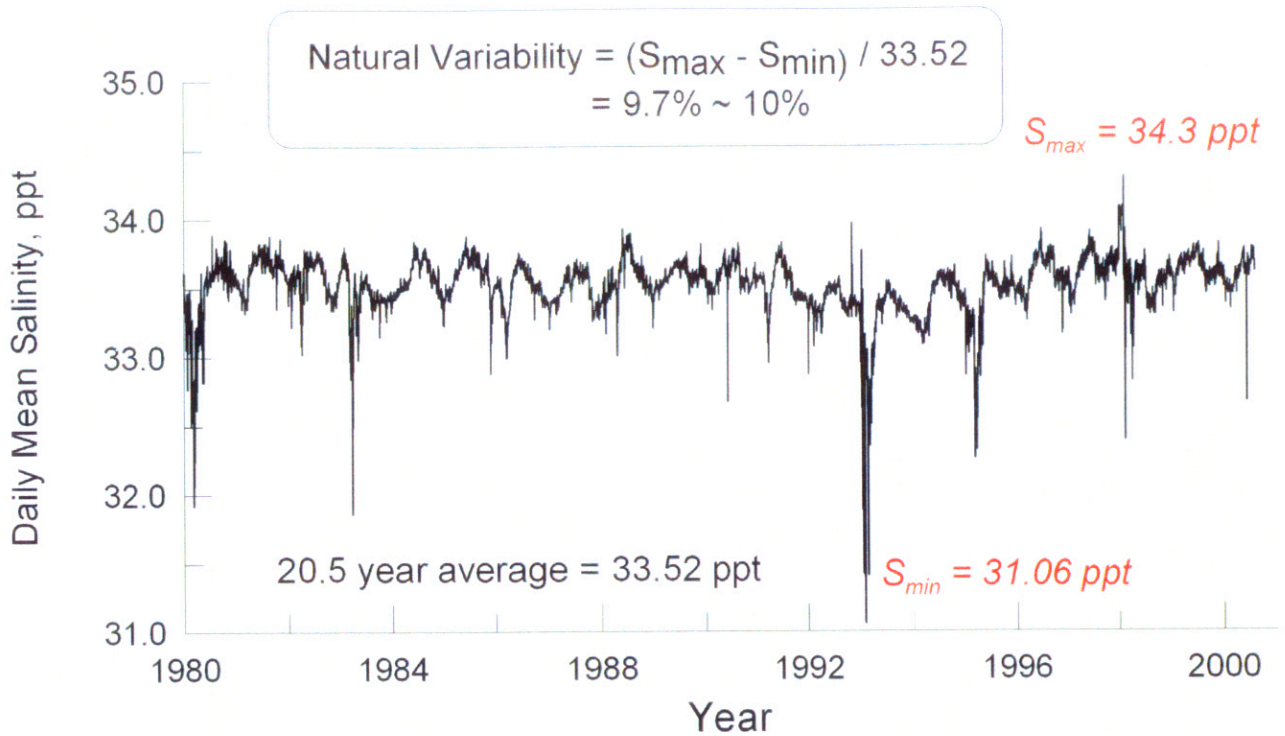


**Figure 2a.** Period of record for ocean water daily mean salinity, Huntington Beach, 1980-2000. [data from NPDES monitoring reports for AES and OCSD outfalls, in MBC, 1980-2001; OCSD, 1993, 2000]

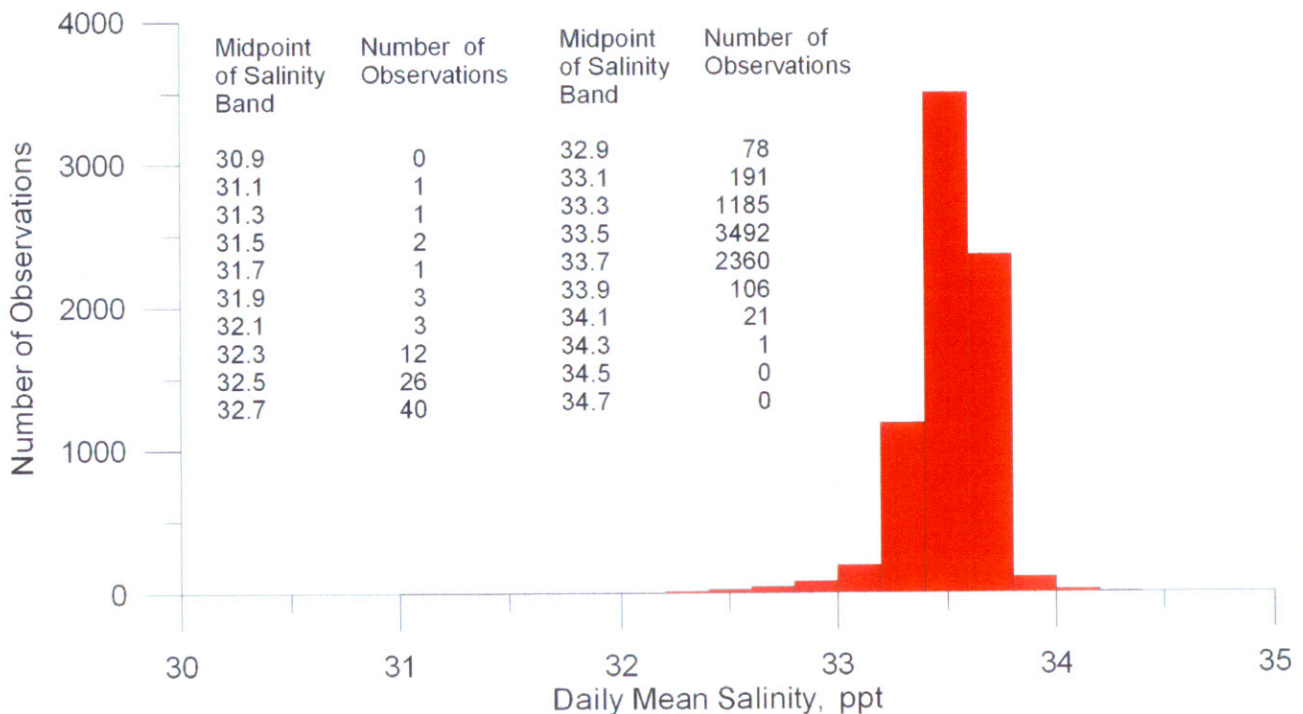


**Figure 3.21.** Histogram of ocean water daily mean salinity, Huntington Beach, 1980-2000. [from MBC, 1980-2001; OCSD, 1993, 2000]

days of the period of record and were below average during 1,543 days. Therefore above average salinities are more common than below average salinities. Average salinities were observed a total of 3,492 days of the period of record, or about 46% of the time. (These data are also confirmed by long term salinity monitoring at Scripps Pier NOAA Station #941-0230, and by 55 CalCOFI cruises in the Southern California Bight between 1984 and 1997, see SIO, 2001; Roemmich, 1989, and Bograd, et al, 2001).

#### **H) Ocean Temperature**

Ocean temperature effects the buoyancy of the combined discharge of the generating station and the desalination plant. The ocean temperature further effects the buoyancy of the discharge through the absolute temperature of the plant discharge, which is regulated under the NPDES permit by a  $\Delta T$  limit relative to ocean temperature. This buoyancy effect is calculated by the specific volume change of the discharge relative to the ambient ocean water according to Equation (5). The buoyancy of the plume exerts a strong effect on the mixing and rate of assimilation of the excess heat and sea salts by the receiving waters.

We use the average of temperature records from NPDES monitoring data along the 8.5 meter depth contour at Stations 8a and 8g to characterize the temperature environment off AES Huntington Beach (see MBC 1980-2002, NPDES Monitoring Reports). We use the average of these 2 stations to avoid aliasing from the thermal plume emitted from the AES outfall at Station 8d. Gaps in the record derived from Stations 8a and 8g were preferentially filled with temperature data from the NPDES monitoring reports of the OCSD outfall (OCSD, 1993,2000). Any remaining gaps were filled from the Scripps Pier Shore Station ( SIO, 2001). The

20.5 year record of daily mean ocean water temperatures is plotted in Panel-c of Figure 3.23 found at the end of this section, summarizing the complete set of boundary conditions. A pronounced seasonal variation in these temperatures is quite evident with the maximum recorded daily mean temperature reaching 25.1 °C during the summer of the 1993 El Niño and the minimum falling to 9.9 °C during the winter of the 1999-2000 La Niña. The 20.5 year mean temperature was found to be 17.6 °C. On a percentage basis, the natural variability of the temperature of coastal waters in the vicinity of AES Huntington Beach Generating station is significantly greater than that of salinity (on the order of  $\Delta T = 86\%$  vs  $\Delta S = 10\%$ ).

#### **I) HBGS Operating Temperatures**

California's Thermal Plan incorporates provisions of Section 316(a) of the Federal Water Pollution Control Act of 1972 and defines the relevant regulatory requirements for cooling water discharge from the AES Huntington Beach Generating station. Although certified to discharge thermal waste at as much as 30 °F (16.5 °C) above ambient ocean temperatures, ( $\Delta T = \Delta T = 30$  °F), the AES plant operators have adopted operating procedures that discharge considerably below the maximum certified Delta-T. NPDES monitoring data from MBC (1980-2002) show that the plant discharge temperatures track the ambient ocean temperatures rather clearly with an average Delta-T of 18 °F (10 °C). This value is used for modeling marine environmental effects due to desalination during normal electrical generation activities. The discharge temperatures occasionally spike to as high as 113 °F(45 °C) during short term heat treatment cycles performed to remove bio-fouling from the cooling water circulation system. (NPDES permit constraints limit heat treatments to a maximum of 125 °F). Since the desalination plant will not

operate during heat treatments, the heat treatment temperature spikes are neglected in the analysis. Regardless, high discharge temperatures promote rapid mixing and assimilation of the excess sea salts from desalination by reducing the negative density anomaly caused by the heavy brine. Therefore, we include in this study model results for “cold water” discharges (Delta-T of 0 °F ) during *standby mode* when **two** circulation pumps are operating but the generating station is not operating it’s boilers to produce electricity.

#### **J) Plant Flow Rates and Concentrated Sea Water Discharge Salinity**

Generating station flow rates determine the volume of water available in-the-pipe to dilute the concentrated seawater discharge from the desalination plant. For example, if the ocean salinity is an average of 33.52 ppt then the RO unit will increase the salinity of the plant discharge to as much as 55.37 ppt if only one generating unit is operational, or as little as 37.19 ppt if all four generation units are operating, (Jenkins and Wasyl, 2001). Hence, the operational patterns of the plant will be an important determinant of the variability of the salinity of the combined discharge once the desalination plant is added to the sea water circulation loop of AES Huntington Beach. For the present study we will use 2 historical flow rate databases; 1) the 20.5 year period from 1980 to mid 2000 that preceded the completion of re-powering of HBGS, and 2) the 1.6 year post re-powering period from 1 January 2002 to 30 July 2003. The operational patterns engendered in these two records reflect both historic user demand for electrical power as well as recent plant equipment up-grades.

There are a total of eight cooling water pumps at AES Huntington Beach, each with a capacity ranging from 44,000 gpm to 46,300 gpm. They are paired two

per power generation unit, and there are four power generation units at the site. Because the pumps are operated in pairs as generating units are brought on-line, the cascade of flow rate is as follows:

Unit 1

2 pumps@44,000 gpm each

Combined Capacity = 88,000 gpm = 126.7 mgd

Units 1 and 2

4 pumps@44,000 gpm each

Combined Capacity = 176,000 gpm = 253.4 mgd

Units 1, 2 and 3

6 pumps@44,000 gpm each

Combined Capacity = 264,000 gpm = 380.2 mgd

Units 1, 2, 3 and 4

8 pumps@44,000 gpm each

Combined Capacity = 352,000 gpm = 506.9 mgd

AES Huntington Beach provided plant flow rate data in daily increments.

Figure 3.22 gives the annual averages of daily flow rates for the period 1979 -2002.

The average flow rate for this 24 year period is 234 mgd and no value is less

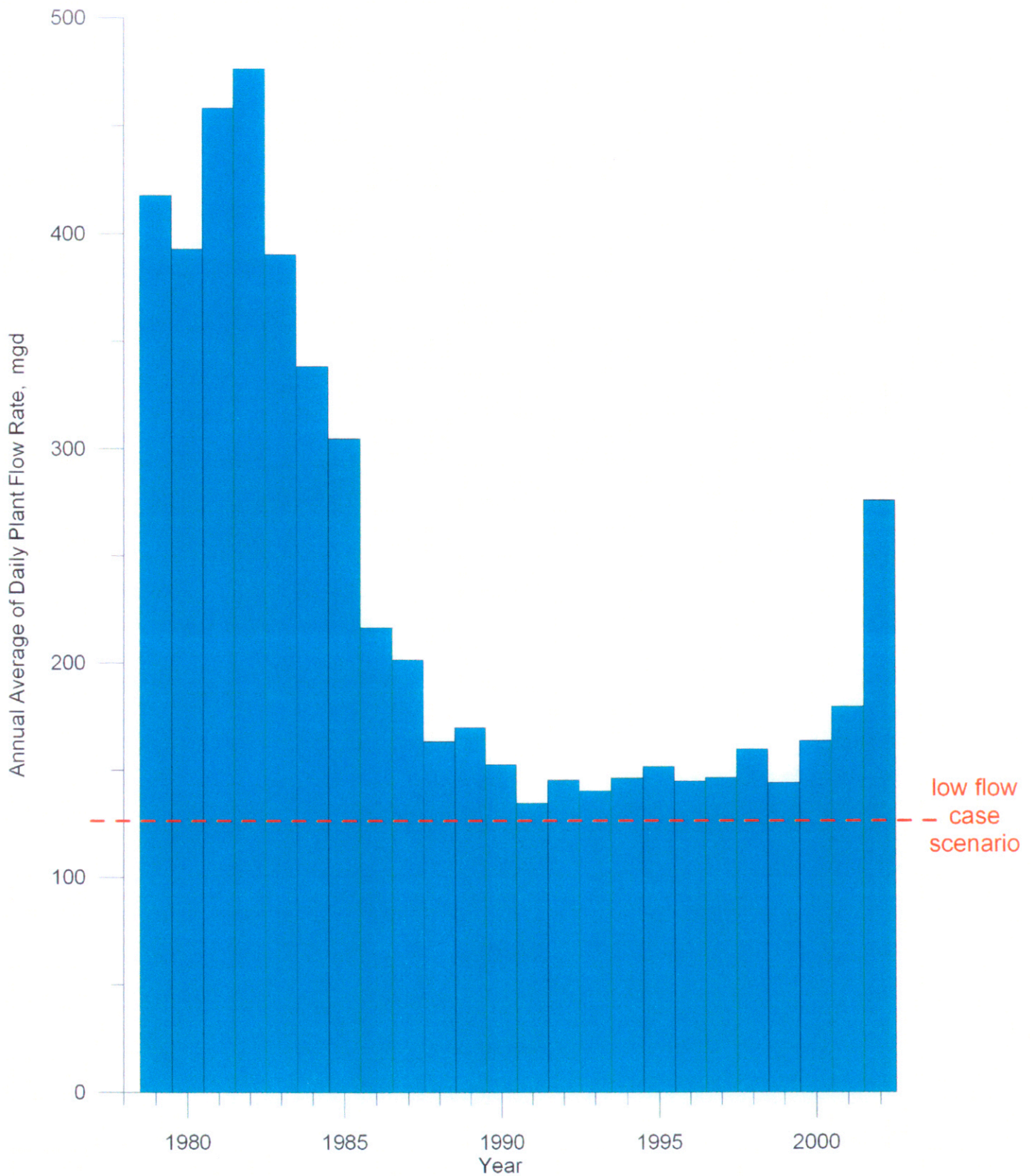


**Figure 3.22.** Annual average of the daily plant flow rate at AES Huntington Beach LLC generating station, 1979-2002. [from NDPES, 2002, courtesy of MBC Applied Environmental]

than the low flow case scenario of 126.7 mgd. The 20.5 year record of daily flow rates is plotted in Panel-a of Figure 3.23, summarizing the complete set of boundary conditions. Average daily flow rate for this model simulation period is 226 mgd. Both of these long term averages reflect a number of low production years from 1987-2000 when several of the generating units were down for equipment modernization. The closest operational scenario to either of these long term averages is 2 generation units to be on-line with cooling water circulation at 176,000 gpm or 253.4 mgd.

The cooling water pumping rate of seawater discharged through the offshore outfall may be supplemented by in-plant waste streams certified up to a maximum daily discharge of 1.66 mgd. These in-plant waste streams are primarily storm water draining off the site having fresh water salinities. The plant storm water is gravity fed into the discharge after the cooling water has past through plant condensers. The cooling water is typically heated to temperatures of 10°C above ambient seawater.

The proposed desalination plant will divert approximately 100 mgd of heated condenser water through a reverse osmosis system (RO) before in-plant waste streams are added to the cooling water discharge. The RO system will produce 50 mgd of product from approximately 100 mgd of cooling water diverted from the condenser cooling stream. The RO system will discharge 50 mgd of concentrated seawater by-product at twice ambient ocean salinity, which is subsequently diluted in the remaining cooling water discharge stream. Based on the pumping rate cascade stated above, the salinities and changes in specific volume of the combined generating station and desalination plant discharges are shown in Table 2. Here the discharge rates through the offshore outfall are listed

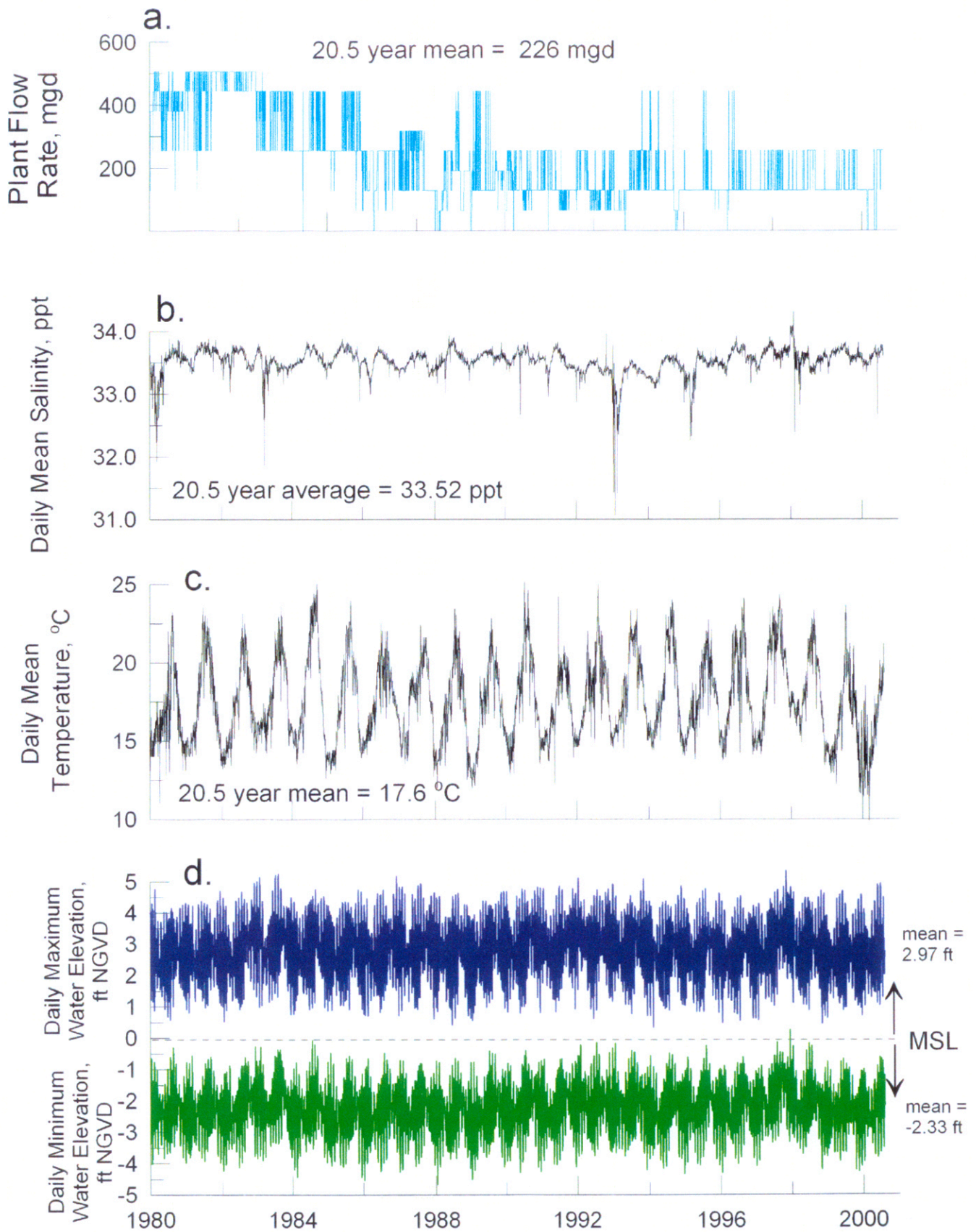


**Figure 3.23.** Controlling environmental variables for brine dilution, boundary conditions: a) plant flow rate b) daily mean salinity, c) daily mean temperature, and d) daily high and low water elevations. [data from MBC, 1980-2001; OCSD, 1993, 2000; SIO, 2001]

without and with supplemental in-plant waste streams in the first and second rows of the table, respectively. In the second row the addition of in-plant waste stream (primarily storm water) is computed at the maximum rate certified under the NPDES permit limits (1.66 mgd). The third row of Table 2 lists the salinity of the discharge if a 50 mgd RO production plant was retrofitted to the cooling water stream leaving the plant condenser. No additional in-plant streams are considered in the row 3 computation, typical of dry weather summer conditions. We find that the RO unit will increase the salinity of the plant discharge to a maximum of 55.37 ppt if only one generating unit is operational (or is in standby mode with 2 pumps on line), with a minimum saline elevation to 37.19 ppt if all four generation units are operating with 8 pumps on line. In row 5 of Table 2 we find that the addition of plant storm water to the combined discharge of the generating station and RO unit will lower the maximum salinities with one generating unit operation by about one part per thousand, or a combined discharge salinity maximum of 54.19 ppt. For all other levels of power generation, the plant storm water has little effect in diluting the concentrated seawater by-product of the RO plant. The end-of pipe discharge salinity for a 50 mgd RO production plant is shown in Figure 3.25 as a continuous function of generating station flow rate. Operating points for the various possible combinations of generating units are shown by the colored dots.

Regardless of whether or not plant storm water is added to the combined discharge of the generating station and RO unit, we find that the water discharged from the offshore outfall will be heavier than the ambient ocean water. For all levels of in-plant flow rate, Table 2 shows that the changes in the specific volume of the discharge due to the addition of the RO unit is always negative.

**Table 2. AES Huntington Beach Discharge Rates and Effluent Physical Properties for Desalination Plant Retrofit**

Generation Units On-Line	1 or standby	1, 2	1, 2, 3	1, 2, 3, 4
Cooling Water Flow Rate (mgd)	126.7	253.4	380.2	506.9
Combined Cooling Water & Plant Storm Water Discharge Maximum (mgd)	128.4	255.1	381.9	508.6
* Salinity (ppt) of Discharge@RO = 50 mgd Plant Storm Water = 0 mgd	55.37	41.76	38.57	37.19
* Specific Volume Change ( $d\alpha / \alpha$ )@RO = 50 mgd Plant Storm Water = 0 mgd $\Delta T = 10\text{ C}$	-0.01592	-0.00472	-0.00210	-0.00096
* Salinity (ppt) of Discharge@RO = 50 mgd Plant Storm Water = 1.66 mgd	54.19	41.42	38.38	37.05
* Specific Volume Change ( $d\alpha / \alpha$ )@RO = 50 mgd Plant Storm Water = 1.66 mgd $\Delta T = 10^\circ\text{C}$	-0.01494	-0.00444	-0.00194	-0.00085

\* Based on an annual mean local ocean salinity of 33.52 ppt

Consequently, the discharge water will sink to the seafloor after the initial vertical momentum of the discharge has diffused into the water column. This has several positive implications: 1) it will increase initial dilution of the combined discharge, 2) it will remove the majority of the thermal footprint from the sea surface, and 3) it should diminish the size of the thermal footprint. Sinking of the discharge plume to the seafloor after the initial vertically upward discharge from the outfall tower will produce trajectories of the effluent that engage the entire water column in the

dilution process. These trajectories should increase initial dilution. Subsidence of the discharge plume to the seafloor following this higher initial dilution should isolate both the concentrated seawater and the waste field of the generating station from subsequent ingestion by the infall tower at mid-water column depths (the infall draws water from 4.8 m (15.8 ft) above the bottom). This is a favorable circumstance with respect to re-circulation. On the other hand, the heavier than seawater discharge plume will bring the elevated salinities into contact with the seafloor where there could be an effect on benthic biology. The extent of seabed effected in this way is studied in Section 4.

#### **K) Event Scenarios Derived From Historical Data 1980-2000**

Overlapping 20.5 year long records of the 4 primary boundary condition variables: generating station flow rates (Figure 3.23a), ocean salinity (Figure 3.23b), ocean temperature (Figure 3.23c), and ocean water levels (Figure 3.23d). Coincident records for the 3 primary forcing functions are shown in Figure 3.24 for waves, currents and winds. These records contain 7,523 consecutive days between 1980 and 2000. We adopt a commonly used approach in environmental sciences for bracketing the variability of long period records with event scenarios of historically worst day, average day, worst month and average month conditions. The criteria for a worst day and worst month was based on the simultaneous occurrence of seven variables having the highest combination of absolute salinity and temperature during periods of low plant flow rates concurrent with low mixing and advection in the local ocean environment. The worst day and worst month involve some potential situations for operating the desalination plant when the

generating station is not generating electricity in standby mode or when it is operating at very low production levels. We refer to these as “theoretical extreme low flow cases” because they are caused by extreme conditions occurring “in-the-pipe” in combination with extreme conditions in the ocean environment. These theoretical extreme low flow conditions (abbreviated “*low flow cases*”) are superimposed on the historic extreme combinations of the remaining 6 controlling variables in Figures 3.23 and 3.24. The resulting modeled response gives the expected impacts for a set of theoretical low flow cases that can not be reproduced from the historic records of all 7 controlling variables during last two decades (1980- July 2000). To establish a statistical comparison for these theoretical extreme cases, we subsequently develop 7523 alternative solutions in Section 5 for the modeled ocean response to the 50 mgd desalination plant, based on historically realized plant operations and ocean conditions. Criteria for low flow case conditions are summarized in Table 3 below.

In the low flow scenarios, brine concentration from the desalination plant is maximized when the AES flow rate is at the minimum operational level (sufficient for power generation) while the ocean salinity is maximum. The low flow case scenario is based on the minimum AES generating configuration or a standby mode with two circulation pumps on line. This configuration involves an in-plant flow rate of 126.7 million gallons per day (mgd). The desalination plant must have at least 100 mgd of in-plant flow available to make 50 mgd of product water, and no combination of HBGS pumps can meet this requirement at less than 126.7 mgd. Consequently, minimum operational flow rate for the desalination plant is limited to no less than 126.7 mgd, and production of product water would cease for any flow rate less than 126.7 mgd.

**Table 3: Search Criteria and Ecological Significance for Low flow Case Combinations of Controlling Variables.**

Variable	Search Criteria	Ecological Significance
Plant Flow Rate	Minimize	Lower flow rate results in less initial dilution in the pipe of the concentrated sea salts from desalination
Ocean Salinity	Maximize	Higher salinity leads to higher initial concentrations of sea salts in the pipe from desalination
Ocean Temperature	Maximize	Higher temperature leads to greater stress on resident marine biology
Ocean Water Levels	Minimize	Lower water levels result in less dilution volume in the nearshore and consequently slower dilution rates
Waves	Minimize	Smaller waves result in less mixing in surfzone and less inshore dilution
Currents	Minimize	Weaker currents result in less advection and less offshore dilution
Winds	Minimize	Weaker winds result in less surface mixing and less dilution in both the inshore and offshore

The minimum operational flow rate provides the least amount of “in-the-pipe” dilution and the highest brine concentrations that would be discharged from the desalination plant and consequently represents the worst *possible* case. The histogram in Figure 3.22 shows that AES Huntington Beach has not averaged daily flow rate less than the low flow case modeling condition during any year in the period of record.

Minimum ocean mixing levels were obtained from a computer search of 20 year long records of winds, waves and currents, (as detailed in Jenkins and Wasyl,

2001 and in the technical appendix of the EIR). The red dashed line in Figure 3.24 identifies the time in these records when waves, currents and winds were simultaneously at a minimum. However, the ocean salinity at this time was 33.52 ppt, not the salinity maximum of 34.3 ppt identified in Figure 3.21a. This is due to the fact that salinity maximums are mutually exclusive with mixing minimums. Salinity maximums are caused by vigorous southerly winds that create a well-mixed coastal ocean while pushing high salinity water masses into the Southern California Bight. A series of sensitivity analyses determined the salinity maximum would increase the concentration of brine discharge by 2%, but that the effects of this increase on brine dilution were smaller than the dilution impairment caused by the effects of retarded mixing during low energy conditions . In fact the dilution rates for the conditions are 99% smaller than the dilution rates during the salinity maximum in Figure 3.21a, (see Section 4). Therefore, minimal ocean mixing conditions became the dominant set of environmental variables in defining the low flow case scenario. Accordingly low flow case dilution modeling was based on the following set of parameters:

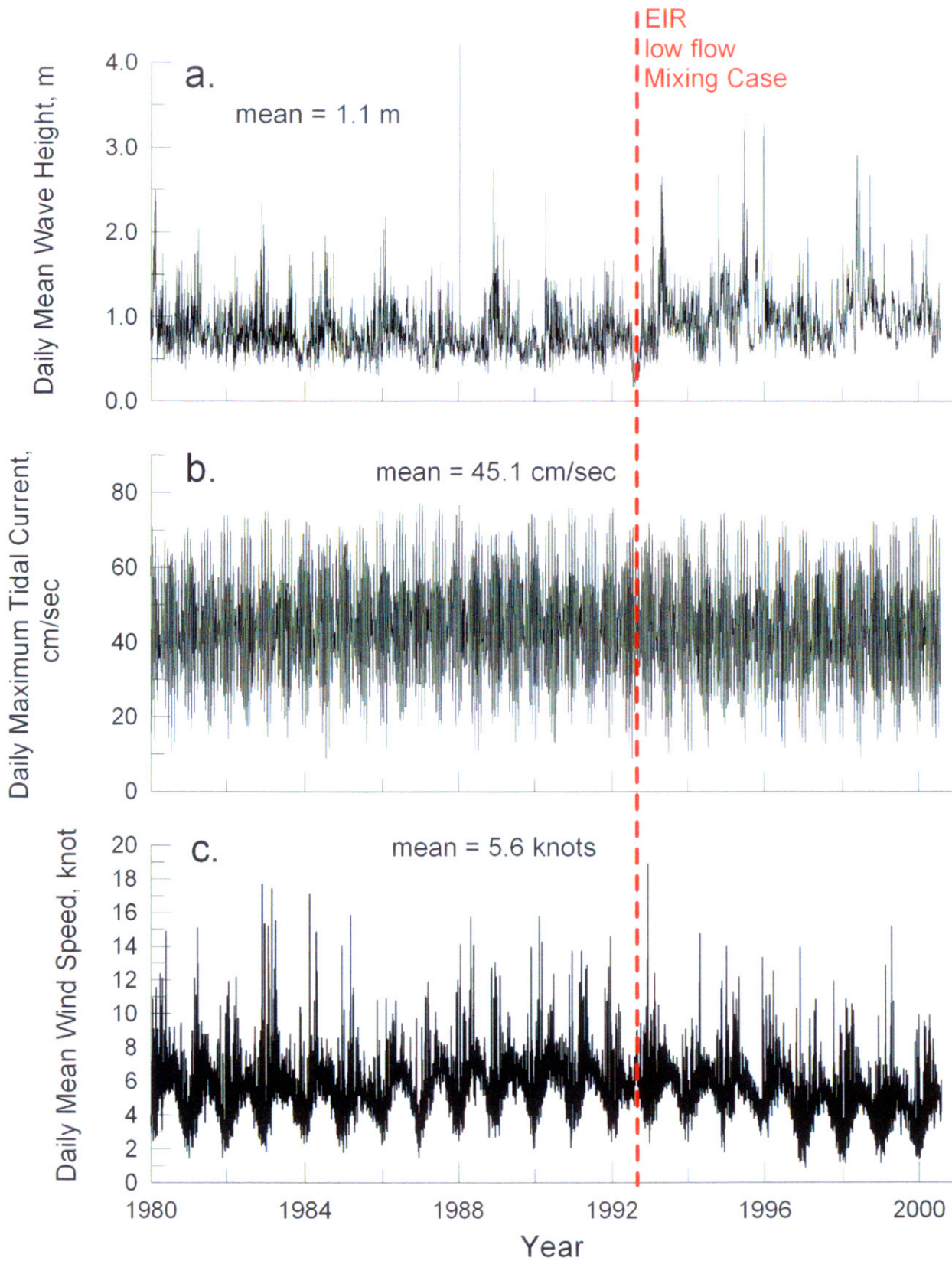


**Figure 3.24.** A 20.5 year record of forcing for the Newport Littoral Cell [centered at Huntington Beach, CA]. a) daily mean wave height (CDIP), b) daily maximum tidal current velocity (Station 8d), and c) daily mean wind (Station 8d). [data from CDIP, 2001; SIO, 2001; NCDC, 2004]

**Table 4: Input Parameters for Low flow Case Simulations**

- 1) AES intake flow rate = 126.7 mgd
- 2) Desalination production rate = 50 mgd
- 3) Combined discharge = 76.7 mgd
- 4) Ocean salinity = 33.52 ppt
- 5) End-of pipe combined discharge salinity = 55.37 ppt
- 6) Combined discharge temperature anomaly  $\Delta T = 10^0$  C
- 7) Combine discharge density anomaly  $\Delta\rho/\rho = 1.59$  %
- 8) Wave height = 0.16 m
- 9) Wave period = 8 sec
- 10) Wave direction =  $255^0$
- 11) Wind = 0 knots
- 12) Tidal range = Syzygian spring/neap cycle
- 13) Daily maximum tidal current = 8.7 cm/sec

Ocean conditions represented by these parameter assignments did not persist in the long term record of Figure 3.24 for more than a week. However, in the model simulations these conditions were perpetuated for 30 days to verify the stability of the computed results as well as specify a low flow month scenario. Historically, the recurrence of low flow case environmental extremes is about 1 week every 3 to 7 years, commensurate with the dominant ENSO frequencies. By perpetuating low flow case conditions in the model for 30 continuous days the recurrence interval is actually more rare, about 1 month every 13 to 31 years.

The average day and average month scenarios were found by a statistical search of these records for the average 24 hour and 30 day combinations

of the 7 variables occurring over the 20.5 year period of record. This procedure produced the model scenarios presented in the EIR. Based on analysis of the AES plant operations data (Figures 3.22) and the ocean monitoring data (Figures 3.23 & 3.24), the following parameter assignments were made for average case dilution modeling:

**Table 5: Input Parameters for Average Case Simulations**

- 1) AES intake flow rate = 253.4 mgd
- 2) Desalination production rate = 50 mgd
- 3) Combined discharge = 203.4 mgd
- 4) Ocean salinity = 33.52 ppt
- 5) End-of pipe combined discharge salinity = 41.42 ppt
- 6) Combined discharge temperature anomaly  $\Delta T = 10^{\circ} \text{C}$
- 7) Combine discharge density anomaly  $\Delta \rho / \rho = 0.44 \%$
- 8) Wave height = 1.1 m
- 9) Wave period = 11 sec
- 10) Wave direction =  $267^{\circ}$
- 11) Wind = 5 knots
- 12) Tidal range = Syzygian spring/neap cycle
- 13) Daily maximum tidal current = 45.1 cm/sec

In Section 5 we augment the event analysis with continuous modeling simulations on the entire set of 7,523 daily combinations of the 7 controlling variables in the 1980-mid 2000 period of record. This is period was selected

because it is the longest length of time for which an uninterrupted record of directional wave data can be assembled in this region. The purpose of this long-term continuous modeling exercise was to both establish the viability of the EIR procedure as well as examine the persistence of all the intermediate outcomes occurring between low flow and average cases. In addition changes to the dispersion statistics of the hyper-saline plume are examined for cold water discharges from AES Huntington Beach, as a consequence of the generating station pumping seawater at 126.7 mgd with a  $\Delta T = 0$ .

#### L) Calibration

The coupled sets of models shown in Figure 2.1 were calibrated for end-to-end simulations of the salinity and temperature fields based on salinity and temperature depth profile measurements conducted over a nearshore sampling grid during November and December 2000 by MBC (2001). These measurements are listed in tabular form in Appendix H together with a sampling map and were collected as part of an NPDES compliance monitoring program for AES Huntington Beach. Wave and current forcing for the model were reconstructed for this two month period based on the wave data in Figure 3.9 and tidal current reconstructions like those in Figures 3.13 to 3.20. Free parameters in the subroutines were adjusted iteratively until a best fit was achieved between the measured and simulated salinity fields.

The subroutines of **SEDXPORT-f** contain seven free parameters which are selected by a calibration data set specific to the coastal type for which the hindcast simulation is run. These parameters are as follows according to subroutine:

**BOTXPORT-f**

\*ak2 - stretching factor for vertical eddy diffusivity,  $\epsilon$

\*ak - adjusts mixing lengths for outfalls

#### NULLPOINT.f

\*ak7 - adjusts the asymmetry of the bedform distribution curve,  
 $\mu$

#### SURXPORT.f

\*aks - adjusts the surf zone suspended load efficiency,  $K_s$

ak4 - stretching factor for the horizontal eddy diffusivity,  $\epsilon_x$

#### RIVXPORT.f

\*ak3\_1 - adjusts the jetty mixing length and outfall mixing  
lengths

\*ak3 - stretching factor for the horizontal eddy diffusivity  
of the river plume,  $\epsilon_H$

The set of calibration values for these parameters was used without variation or modification for all model scenarios contained in Sections 4-9.